Pergamon

Geochimica et Cosmochimica Acta, Vol. 62, No. 7, pp. 1175–1193, 1998

0016-7037/98 $19.00 + .00

PII S0016-7037(98)00047-7

Ion microprobe study of plagioclase-basalt partition experiments at natural concentration levels of trace elements

ILYA N. BINDEMAN,[1,*] ANDREW M. DAVIS,[2] and MICHAEL J. DRAKE[3]

[1]Department of the Geophysical Sciences, University of Chicago, Chicago, Illinois 60637, USA
[2]Enrico Fermi Institute, University of Chicago, Chicago, Illinois 60637, USA
[3]Lunar and Planetary Laboratory, University of Arizona, Tucson, Arizona 85721, USA

(*Received February* 3, 1997; *accepted in revised form December* 12, 1997)

Abstract—We present here a study of plagioclase/melt partitioning of trace elements at their natural concentration levels, using sample charges from the widely cited plagioclase/melt partitioning experiments of Drake and Weill (1975). In these experiments, sample charges were doped to ~1 wt% with Sr, Ba, rare earth elements (REE) and Y, but each charge was only doped with one to four elements. Thus, these samples provide an opportunity to compare partition coefficients (D_i) at natural concentration levels with those for doped concentration levels for the same composition of plagioclase, melt and temperature. Plagioclase-glass pairs of seventeen runs at four different plagioclase compositions and temperatures were analyzed by electron microprobe for major elements and some of the doped trace elements and by ion microprobe for undoped Li, Be, B, F, Mg, P, Cl, K, Sc, Ti, V, Cr, Mn, Fe, Co, Ni, Rb, Sr, Y, Zr, Nb, Cs, Ba, La, Ce, Pr, Nd, Sm, Eu, and Pb. Partitioning of the homovalent substituting ions Sr^{2+} and Ba^{2+} show no differences between doped and natural concentration levels. Ion microprobe measured D_i heterovalent substituting ions REE^{3+} and Y^{3+} at natural concentration levels (0.3–3 ppm) in samples doped with wt% levels of Sr or Ba are up to three times higher than at doped concentration levels and cannot be explained by analytical artifacts. We discuss possible reasons for this.

All trace element D_i data show linear relationships of the forms $\ln (D_i) = a^* X_{An} + b^*$ and $RT \ln (D_i) = a X_{An} + b$ in $0.4 < X_{An} < 0.8$ range. Alkalies, alkaline earths, and lanthanides exhibit the same type of compositional dependence within each group of elements. Slopes a^* and a vary with the increase of the ionic radius within each valence group. The smaller ions of each of these groups exhibit no or positive slopes a^* and a; the larger ions show negative slopes. The magnitudes of the slopes increase linearly with ionic radii within the same valence group. This relationship allows extrapolation and prediction of the compositional dependence of elements of the same group whose concentrations could not be measured in this work.

We present best fit approximation parameters for the $RT \ln (D_i) = a X_{An} + b$ relationship. These can be used in various petrologic applications to reconstruct the primary trace elemental composition of the parental melt from which plagioclase crystallized. *Copyright © 1998 Elsevier Science Ltd*

1. INTRODUCTION

Partition coefficients of trace elements between different igneous minerals and melts are widely used in geochemical and petrological applications, such as modeling of melt evolution through fractionation, partial melting, or mixing (e.g., McKay, 1989), and reconstruction of primary melt composition via trace element concentrations in liquidus phases (Blundy and Shimizu, 1991; Singer et al., 1995; Papike et al., 1995, 1996; Bindeman et al., 1998).

Plagioclase is one of the most important minerals in these studies because it is present as a liquidus phase in many terrestrial and lunar magmas (Phinney, 1992), as well as in some meteoritic melts (Stolper, 1975; Beckett and Grossman, 1988). Plagioclase has several important advantages over other minerals (e.g., pyroxenes). The slow character of CaAl-NaSi interchange in plagioclase makes it a good candidate for retention of its original crystallized trace element contents. Morse (1984) has demonstrated that 1 μm-scale magmatic oscillatory zoning of plagioclase is preserved in Archean anorthosites. Recent experiments of Giletti (1994) and Giletti and Casserly (1994) showed that plagioclase has very slow diffusivities of major components and high closure temperatures. Diffusivities of trace elements are 1–4 orders of magnitude slower and decrease with increasing charge and size of trace element cations (Giletti, 1994). In addition, natural plagioclase has concentrations of a number of trace elements that are easily measured by ion microprobe.

Until recently, the only way to experimentally determine D_i, the ratio of concentrations by weight in mineral and melt, was by doping the system with wt% levels of trace elements to enable electron microprobe analyses of coexisting mineral and glass. Drake (1972) added 0.2–3 wt% levels of REE, Y, Sr. and Ba to natural and synthetic basaltic compositions. Plagioclase and glass were subsequently analyzed by the electron microprobe to obtain D_i in the An_{40}–An_{80} compositional range (Drake and Weill, 1975). Weill and McKay (1976) and McKay and Weill (1977) extended the range of these experiments to An_{92}-An_{97} in similar experiments. Simon et al. (1994) and Blundy and Wood (1994) presented D_i for An_{97} and An_{89}, respectively. Many experimentally determined D_i exist for Sr and Ba (for a review, see Blundy and Wood, 1991).

Questions have been raised previously about the applicability of wt% level doping experiments to the natural situation in which trace elements are at the ppm level (Mysen, 1978;

* Author to whom correspondence should be addressed (inbindem@midway.uchicago.edu).

Table 1. Experimental conditions and products of analyzed runs.

RUN	T °K	System	Doped element	X_{An}, Avg %	% crystals	Crystal width, μm
91-3	1570	MP1+40% An	Sr	76.1	30	60
91-4	1570	MP1+40% An	Sr	77.2		60
92-1	1523	MP1+10% An	Sr	67.7	12	50
92-2	1523	MP1+10% An	Sr	65.4	15	50
87-1	1463	MP1+20% Ab	Sr	51.0		25
87-5	1463	MP1+20% Ab	Sr	57.3	22	22
94-3	1426	MP1+50% Ab	Sr	42.6	18	15
94-5	1426	MP1+50% Ab	Ba	44.8	20	10
94-7	1426	MP1+50% Ab	La	44.7	16	18
S-2	1570	$Ab_{42.5}An_{42.5}Di_{15}$	Sr	67.4	20	40
S-3	1570	$Ab_{42.5}An_{42.5}Di_{15}$	Sr	71.2	15	40
99-5	1460	MP1+20% Ab	La,Ce,Y,Lu	52.5	25	20
99-7	1460	MP1+20% Ab	Nd, Dy, Er	53		20
99-2	1460	MP1+20% Ab	Sm, Eu,Gd	53		20
101-4	1572	MP1+40% An	La,Ce,Y,Lu	75.5		50
101-3	1572	MP1+40% An	Sm,Eu,Dy	75		50
101-7	1572	MP1+40% An	Nd,Dy,Er	75		50

MP1 is a natural basaltic andesite from Mountain Pass, Oregon; Ab, An, Di are synthetic albite, anorthite and diopside (see Table 1 in Drake and Weill, 1975, for analyses). X_{An} was measured on the University of Chicago electron probe in 1996. % of crystallization for selected runs is determined by image analysis of SEM backscattered electron images. Crystal size refers to the width (minimal dimension) of an average plagioclase grain.

Beattie, 1993). The beta-track method, in which charges are doped with a beta-emitting radioactive isotope of the element of interest, has been used to check the relationship between D_i and concentration down to the 1 ppm level (Hoover, 1978; Drake and Holloway, 1978). For example, Harrison and Wood (1980) showed that ^{151}Sm substituted into defect sites in high purity pyrope at concentrations below 1 ppm. However, Beattie (1993) used the ion microprobe on the same samples to show that their result was an analytical artifact, probably resulting from the production of several tracks from a single beta particle. Beattie (1993) showed that Henrian behavior was obeyed from sub-ppm to several wt% concentration levels, until the concentration of Sm became high enough to stabilize Sm-garnet.

The ion microprobe technique provides a reliable method of measuring D_i for trace elements at their natural concentration levels. Here we present a systematic application of the ion microprobe to plagioclase-basaltic melt partitioning. It is important, therefore, to compare these new results with previous measurements made by the electron microprobe at wt% concentration levels. The widely cited doped experiments of Drake and Weill (1975) provide an excellent set of samples for such a study because of the opportunity to compare partition coefficients at natural concentration levels with those for doped concentration levels for identical compositions and temperatures. We report here ion microprobe analyses of many Drake and Weill (1975) sample charges for thirty different undoped trace elements and a few of the doped ones.

2. EXPERIMENTAL PROCEDURE AND RUN PRODUCTS

The experiments on which this work is based were conducted over twenty-five years ago in furnaces in air at 1 atm total pressure. In these experiments, various proportions of synthetic albite and anorthite were added to a natural basaltic andesite to ensure that plagioclase is the only mineral crystallizing from the melt. The reader can find a detailed description of experimental conditions and starting compositions in Drake and Weill (1975) and Drake (1972). Table 1 summarizes conditions for runs which were reanalyzed in this study. Major and trace element compositions of starting material MP1 and a synthetic albitic glasses are given in Table 2. We were not able to locate the starting synthetic anorthite and diopside used in these runs 25 years ago. The synthetic albite glass contains measurable quantities of some trace elements; the same may be true of other synthetic materials used in experiments.

The experiments of Drake (1972) were done as follows. The starting mixtures of MP1 glass and synthetic albite, anorthite, and diopside glasses plus some doped elements were placed in 2 mm diameter platinum capsules. The capsules were then sealed and held ~150° above the liquidus for 1.5–8 h to provide melting and homogenization. Because plagioclase is a difficult mineral to nucleate and grow experimentally, it took many tries and experimentation to learn how to nucleate and grow homogeneous crystals. The developed procedure included stepwise cooling from the above the liquidus temperature to the temperature of interest for 0.5–1 h to nucleate and grow plagioclase. Samples were held at the required temperature for 1 week to ensure complete trace element equilibration between plagioclase and melt.

Backscattered electron imaging of run products with a scanning electron microscope shows that plagioclase was the only liquidus mineral in all runs. The proportion of crystals is in the range 10–25 vol%. Plagioclase is represented by the highly elongated (1:5–1:30) noodle-like crystals, often with hollow interiors (Fig. 1). This morphology is consistent with rapid growth of plagioclase (e.g., Lofgren, 1974) and probably reflects the first stages of cooling from above to below the liquidus. The one-week long equilibration time seems to be incapable of changing this morphological birthmark of the crystals. The elongated and skeletal morphology of the crystals provides a large plagioclase surface area, favoring effective trace element exchange between each crystal and the surrounding melt. Crystal width decreases with decrease of temperature and increase of viscosity of the melt (see Table 1).

3. ANALYTICAL TECHNIQUES

Epoxy mounts of experimental products were polished with 1 μm diamond paste and then etched for 30 s with fluoboric acid. Etching enhances relief in reflected light by preferentially dissolving grain boundaries, cracks, glass, and melt inclusions. It enables a correct optical identification of ion microprobe spots for analysis. Etched surfaces were then polished again for a short time to ensure that no surface contamination remains as a result of etching.

Present-day imaging techniques give better visual control over the choice of spots for analyses than was possible 25 years ago. Run products were first studied under reflected light and then with secondary and backscattered electron imaging on a JEOL JSM-5800LV scanning electron microscope (SEM) at the University of Chicago. We reanalyzed the run products listed in Table 1 by electron microprobe, including profiling of some crystals with respect to major elements to ensure the absence of zoning of each crystal and homogeneity of different crystals within each run product. Wavelength-dispersive analyses were made on a Cameca SX-50 electron microprobe using an accelerating voltage of 15 kV. Standards of Amelia albite, synthetic anorthite glass, and synthetic plagioclase glass of intermediate composition were used for major element calibration. Several synthetic glasses, doped with 4 wt% each of several REE (Drake and Weill, 1972), were used as standards for new electron microprobe REE analyses of some of the doped samples of Drake (1972).

We used a 1 μm diameter beam for 1 μm-step profiling through the crystals to check for homogeneity. In contrast, a 15 μm diameter beam was used to analyze and compare different crystals and glass for homogeneity. The larger diameter of the beam also minimized sodium loss during analyses of Na-rich samples.

Samples which were imaged with the SEM and analyzed by electron microprobe were analyzed later by ion microprobe. This makes possible a comparison between electron and ion microprobe measurements. Ion microprobe analyses were made using a modified AEI IM-20 instrument at the University of Chicago. The analytical techniques used are similar to those described in Hinton et al. (1988), Davis et al. (1991), Bindeman (1998), and MacPherson and Davis (1993, 1994). Molecular interferences were reduced by energy-filtering. The AEI IM-20 is quite different in design from the Cameca ims-3f series instruments commonly used for trace element analysis; the degree of energy filtering used on the AEI corresponds to an 80–100V offset on a Cameca ion microprobe. Molecular interferences, such as $^{29}Si^{16}O^{+}$ on $^{45}Sc^{+}$ or light REE oxides on heavy REE, were corrected for based on measurements of interference-free molecular peaks and on measurements of molecular interferences in many standards. Calcium-normalized ion yields were obtained from a variety of natural and synthetic silicate standards. Previous experience has shown that there is little variation of ion yields in different silicate matrices under the energy-filtering conditions used in this work. One exception to this is Si, which has significant matrix effects. For this reason, we adjusted the ion yield for silicon such that the SiO_2 content matched the electron microprobe value for glasses and matched the amount calculated from feldspar stoichiometry for plagioclase. For each sample, six cycles through the mass peaks were made, so that we could monitor whether the primary beam sputtered into a melt inclusion or into adjacent glass during analysis of plagioclase.

Ion microprobe analyses for concentrations of a variety of undoped elements in most of the runs (see Table 1) were made on the Sr-doped series, because Sr caused no isobaric interferences with other ions. We also analyzed seven REE-doped and Y-doped samples in order to determine partition coefficients of Sr at natural concentration levels and to compare results with the electron microprobe measurements of REE and Y of Drake (1972). Several new electron microprobe analyses for REE and Y were also made. Therefore, altogether, we analyzed 9 Sr-doped samples, 1 Ba-doped sample, 1 La-doped sample, and 2 each of the La-Ce-Y-Lu-doped, Sm-Eu-Gd-doped, and Nd-Dy-Er-doped sample series (Tables 2 and 3).

The small size of the crystals (15–60 μm) and the relatively large diameter of the ion beam (~10 μm) required consideration of the possibility of plagioclase contamination from adjacent glass in each analysis and made it necessary to discard some analyses. Several criteria were used to do this. The sputtering history of each spot was checked for absence of increase in concentrations of some incompatible trace elements, which would result from glass contamination. Each of the ion microprobe sputter pits was later studied by SEM to ensure that there has been no lateral overlap onto adjacent glass. We normally analyzed at least two spots each on plagioclase and glass in each run product (Table 2). Clearly discrepant analyses were rejected.

4. RESULTS

4.1. Electron Microprobe and Ion Microprobe Data Comparison

Table 2a presents averaged plagioclase and glass analyses of each run, compiled after discarding obviously contaminated analyses. We found a close similarity between the electron and ion microprobe analyses for the major elements (e.g., MacPherson and Davis, 1994; Simon et al., 1994). The ratios of these concentrations, D_i, of the major elements Mg, K, Ti, and Fe determined from ion microprobe data are almost indistinguishable from those determined from electron microprobe data.

The results show no significant variation in trace element concentration within or among plagioclase crystals in each run product; the variations of most trace elements do not exceed 5 relative percent. The anorthite composition is constant within ± 1.5 mole % uncertainty. Glass is even more homogeneous. Despite this, systematic ± 2 mole % anorthite differences occur between different runs with the same bulk composition held at the same temperature, but doped differently. Our electron microprobe-measured anorthite content in plagioclase is largely similar to that of Drake (1972), except for some of the Na-rich samples. New data for runs 87 and 94 (Table 1) look more stoichiometric and are 2–3 mole % richer in albite. These new values are used in the later discussion of compositional trends of partitioning of trace elements.

Ion microprobe-measured concentrations of Sr and Ba in plagioclase and the glass and D_{Sr}, D_{Ba} in Sr-doped and Ba-doped samples are coincident with those of Drake and Weill (1975). Concentrations and partition coefficients for the light REE (LREE) La, Ce, Nd, Sm as well as Eu and Gd in two run series determined with the ion microprobe (Table 3) are in very good agreement with the electron microprobe measurements of Drake (1972) (Fig. 2). Concentrations of Dy and Y in plagioclase and D_Y, D_{Dy} are found to be in good agreement with the measurements in Ca-rich samples of Drake (1972), but deviate beyond the analytical error in Na-rich samples. We, thus, included ion microprobe measured D_Y for these Na-rich samples later in this work.

Based on this largely good agreement of ion microprobe measurements with the electron microprobe measurements of Drake (1972), we can exclude the possibility of significant spectral interferences for REE in the results of Drake (1972), which gives us confidence in the accuracy of the Drake and Weill (1975) measurements for Sr, Ba, and LREE.

However, ion microprobe-measured concentrations of Er and Lu in plagioclase and corresponding partition coefficients are factor of 4 to 5 smaller than the electron microprobe measurements of Drake (1972), while the concentrations of these elements in the glass are in reasonable correspondence. The concentrations of Lu and Er in plagioclase in these samples are less than 100 ppm, essentially at the limits of detection of the electron microprobe, and call into question the reliability of the reported measurements. These concentrations, however, are

Table 2a. Average concentrations of trace elements in coexisting glass and plagioclase for run products (see table 1 for experimental conditions).

GLASS

Sample	87-1 gl	87-5 gl	91-3 gl	91-4 gl	92-5 gl	92-2 gl	94-3 gl	94-5 gl	94-7 gl	S2-2 gl	S2-3 gl	MP1	Albite
n	3	3	3	3	3	3	5	1	3	3	4	3	2
Element													
wt%													
SiO_2	62.0	60.0	55.8	55.5	55.5	55.7	62.0	62.0	62.5	56.6	56.6	58.4	68.2
Al_2O_3	16.4	17.5	20.4	20.5	19.0	18.5	16.2	15.3	14.8	21.4	21.8	18.8	18.2
CaO	4.72	5.09	9.04	8.90	7.68	7.88	3.84	3.50	3.40	11.88	11.95	7.40	0.10
Na_2O	6.53	6.70	3.86	3.76	4.47	5.64	8.05	8.28	7.43	5.92	5.78	4.40	12.20
ppm													
Li	9.1	13.8	10.3	10.1	7.3	8.7	14.3	24.3	19.0	16.3	21.0	5.9	<1.2
Be	0.33	0.38	0.22	0.25±0.03	0.23	0.18	0.44±0.03	0.46±0.03	0.47	0.19	0.12±0.01	0.19±0.01	0.06±0.02
B	6.7	6.8±0.4	3.6	5.0±1.1	11.7	8.1	9.2±1.7	8.5	7.4±1.1	6.7±0.4	6.2±0.6	6.3	0.6±0.1
F	172±32	230±22	122±10	188±30	78±25	121±28	117±16	172±24	155±37	148±21	178±55	85±13	60±24
Mg	22542	23702	23321	23447	26292	23830±1484	20307	20674	18732	21114	20900±1418	22190	137
P	843	1142	555	587±34	706	533±37	1253±74	1484	1266	279±111	42±17	860	60±24
Cl	116±31	355±18	96±12	100±8	77±27	76	88±5	137±28	110	96±11	74±7	75±11	150±50
K	7364	8431	7457	6713	7879	8829	6781	6353	6125	115	113	7850	432
Sc	16.7±1.9	24.7±3.0	23.2±4.8	20.4±4.2	20.7±2.8	18.6±3.5	14.0±3.8	13.8±5.0	13.7±4.0	5.1±0.7	2.4±0.9	21±2	<8
Ti	5722	6138	5891	6041	6344	5775	4951	5153	4667	71	67±5	5174	90±9
V	138±23	166±14	127±23	194±17	148±13	105±10	117±17	124±26	116±7	<3	<15	63±21	<12
Cr	129	133±8	134	150±	132	126±12	123	124	107±9	38±3	53±5	110	219
Mn	679±7	696±13	698±7	721±9	833±16	778±58	624±11	684±20	574±7	<10	<3	605±18	31±20
Fe	31009	31817	35366	39567	45321	42373±3156	31692	34471	29498	1204±493	754	47100	7830±480
Co	22.2±1.4	24.5±1.2	29.5±2.3	33.3±0.6	34.2±1.2	43.1±1.9	27.6±1.5	45.0±3.4	26.9±1.1	7.0±1.1	4.0±0.6	55.0	5±2
Ni	22.2±3.7	46.5±31.2	65.3±18.8	65.3±5.6	110.5±12.0	118.7±25.8	77.5±22.5	128.1±33.0	78.5±3.3	37.0±15.7	35.0±3.0	430±22	337±42
Rb	29.5	29.0±1.5	21.4	21.1±1.2	21.7	25.6±1.5	35.7	36.6	30.6	1.3±0.2	1.1±0.1	29.0	1.2±0.6
Sr	**3019**	**867**	**2387**	**1171**	**6067**	**4639**	**2689**	282	264	**3492**	**1760**	388	8±6
Y	16.6	18.0	17.1	17.5	18.3	15.6	14.2	15.1	15.1	1.2±0.5	0.6±0.0	12.2	4.7±0.3
Zr	110.8	123.4	125.2	132.4	122.6	101.3±6.3	89.5	97.2	86.6±5.0	88.1	97.0±7.1	74.0	53±2
Nb	5.47	5.87±0.39	4.56	5.6	5.14±0.26	4.17±0.24	4.08±0.26	4.66±0.32	3.7	0.67±0.12	0.61±0.08	3.2±0.2	0.5±0.2
Cs	2.35±0.19	2.47±0.31	1.09±0.06	0.78±0.1	0.91±0.15	1.41±0.09	4.05±0.18	4.44±0.49	3.07	0.181±0.098	0.059±0.038	2.6±0.2	<0.4
Ba	337	355	351	349	402±26	400±23	293	**7889**	319	10	8	336	32±2
La	11.94	10.8	11.08	11.55	15.27	9.7	8.78±0.48	15.04	**25263±2064**	0.87±0.08	0.87	11.0±0.2	2.3±0.3
Ce	30.26	26.58	26.82	28.21±1.13	37.32	23.59±1.05	20.82	32.14	26.09	1.537	1.912	27	5.0±0.5
Pr	3.50±0.10	3.40±0.10	3.30	3.30±0.20	4.30	2.90±0.20	2.50±0.10	3.90±0.10	3.00±0.10	0.20±0.00	0.30±0.00	3.20	0.7±0.1
Nd	12.51	12.77	16.91	12.82	16.34	12.17	9.92	14.67	11.41	1.05	1.01±0.09	13.2	1.5±0.2
Sm	2.61	3.04	2.76	2.8±0.17	3.96	2.99	2.45	3.11±0.21	2.81±0.17	0.141±0.017	0.184±0.04	3.2	0.33±0.11
Eu	0.75±0.09	0.96±0.04	0.92±0.18	1.01±0.08	1.09±0.06	0.86±0.06	0.77±0.07	±0.64	<0.14	0.31±0.04	0.33±0.04	0.72±0.40	1.9±0.21
Pb	20.0±2.2	19.0	12.7±2.6	16.3±3.4	48.5±4.2	27.3±1.7	52.1±8.8	47.4±5.2	34.4±4.8	9.5	4.6±1.3	13.0	<24

Table 2a. (Continued)

PLAGIOCLASE

Sample	87-1 Pl	87-5 Pl	91-3 Pl	91-4 Pl	92-5 Pl	92-2 Pl	94-3 Pl	94-5 Pl	94-7 Pl	S2-2 Pl	S2-3 Pl
n	3	2	3	3	3	3	3	1	6	3	2
An, %	51.0	57.3	76.1	77.2	67.7	65.4	42.6	44.8	44.7	67.4	71.2
Element											
wt%											
SiO_2	55.3	55.0	48.9	49.0	50.5	50.9	57.3	57.1	57.4	51.0	50.1
Al_2O_3	26.6	26.9	32.2	32.2	30.0	29.2	24.7	24.5	25.0	31.0	31.4
CaO	10.13	10.97	15.14	15.19	13.29	13.63	8.74	9.28	8.62	13.39	14.69
Na_2O	5.70	5.50	2.58	2.56	3.38	3.68	6.67	6.61	6.54	3.67	3.32
ppm											
Li	2.3	3.8	2.5	2.6±0.2	1.8±0.1	1.9±0.1	3.0±0.2	5.9±0.3	4.3	2.6	2.9
Be	0.14±0.03	0.14±0.02	0.12±0.01	0.14±0.01	0.11±0.04	0.06±0.01	0.10±0.03	0.08±0.03	0.13±0.04	0.07±0.00	0.04±0.01
B	1.04±0.63	0.97±0.11	0.21	*1.37±0.64*	1.13±0.39	1.03±0.19	*8.22±1.53*	1.67±0.29	1.25±0.30	1.54	0.63±0.11
F	57±8	324±35	59±14	95±22	66±22	184±23	*570±108*	171±54	190±53	68±2	461±53
Mg	767	919	647	740	1028	946	718	1269	760	941±115	964
P	123±24	92±16	44±8	38±14	51	51±11	202±33	250±48	112±11	28±2	18±16
Cl	52±6	239±39	60±19	43±17	81	58±11	139±31	171±69	100±18	44	104±33
K	963±67	1207	695±46	661	953	881	994	1018	997	20	21
Sc	<1.2	7.7±2.1	1.9±0.6	2.4±2.8	1.7±0.7	<3.2	<13.0	<10.4	4.3	5.1±1.8	3.5±2.0
Ti	437±25	473	323	365±20	412	344	473	576±28	421	14	11±2
V	<1.6	<12.0	<2.8	2.0±4.5	<8.8	<9.0	5.7±20.2	<34.0	<16.4	5.2±0.4	7.3±6.4
Cr	6.00±0.71	6.81±1.13	4.17±0.22	4.38±1.11	7.46	5.71	*23.58±4.83*	9.27±2.80	11.63±2.79	3.99±0.52	5.68±1.16
Mn	<60	<60	<66	<59	21±3	33±13	57±11	<44	<28	<66	<67
Fe	7008	7170	3461±210	4533	8621	9252	9147	10116±524	8248	1325±671	289±232
Co	4.0±1.4	4.2±2.0	4.4±2.6	4.2±3.8	3.1±0.2	9.9±1.8	*28.6±5.9*	9.6±4.1	8.2±1.9	6.4±0.8	6.4±2.6
Ni	11.5±1.2	14.0	10.6±6.1	<8.0	<18.0	14.5±6.5	90.0±23.7	43.3±38.5	34.2±11.6	30.7±7.3	<44.0
Rb	1.39±0.94	1.06±0.42	0.71±0.19	0.76±0.35	0.80±0.13	0.55	<2.98	2.45±0.96	0.56±0.08	<0.66	
Sr	**8138**	**2087**	**3803**	**1841**	**10968**	**8065**	**8292**	1062	992	**5412**	**2543**
Y	1.85	1.00±0.08	0.98±0.15	0.75±0.08	1.29±0.19	1.40±0.30	*4.00±0.67*	*1.75±0.22*	0.85±0.13	2.85±1.81	0.30±0.05
Zr	0.37±0.11	0.45±0.12	0.34±0.09	0.18±0.02	0.68±0.21	0.29±0.02	1.13±0.18	1.23±0.41	0.53±0.11	0.78±0.41	<0.10
Nb	0.13±0.03	0.11±0.07	<0.01	<0.04	0.06±0.03	0.05±0.01	0.34±0.10	<0.22	0.06±0.02	0.06±0.02	<0.08
Cs	<0.02	<0.12	<0.09	<0.08	0.06±0.04	0.15±0.10	0.44±0.30	<1.08	<0.64	<0.11	<0.25
Ba	164±17	105	73±14	79±4	100±17	85	177±12	**5463**	211	4.00	3.00
La	2.83±0.14	2.36±0.17	2.19±0.35	2.50	2.68±0.16	1.91	5.54±0.21	7.38±0.62	**6633**	0.63±0.06	1.00±0.14
Ce	5.23	3.81±0.24	4.19±0.40	4.69±0.25	5.06	3.40	8.47	7.48±0.71	10.80±1.07	1.66	2.10±0.23
Pr	0.60	0.60±0.10	0.50±0.10	0.50±0.10	0.60	0.40	1.10	1.10±0.20	1.10±0.10	0.20±0.10	0.20
Nd	2.48	2.01±0.16	2.60±0.26	1.78±0.19	2.86±0.27	2.86±0.32	4.99	4.04±0.48	3.51±0.46	1.12±0.20	1.00±0.14
Sm	0.47±0.05	0.26±0.14	0.29±0.05	0.35±0.05	0.49±0.09	0.56±0.09	1.06±0.19	0.89±0.24	0.52±0.08	0.96±0.73	0.35±0.09
Eu	0.09±0.06	0.07±0.07	0.12	0.19±0.08	0.07±0.04	<0.04	0.47±0.22	<2.08	0.50±0.17	0.05±0.03	0.06±0.02
Pb	16±4	11±3	11±5	7±3	29±8	8	*270±173*	43±11	*82±20*	7±1	3±2

±1σ is given when it is larger than 5% of the value); upper limits are based on 2σ, bold numbers denote doped concentrations, numbers in italics are either imprecise or are clearly outliers and were not used in further treatment.

Table 2b. Average partition coefficients, D_i, for run products.

Sample	87-1 D	87-5 D	91-3 D	91-4 D	92-5 D	92-2 D	94-3 D	94-5 D	94-7 D	S2-2 D	S2-3 D
An, %	51.0	57.3	76.1	77.2	67.7	65.4	42.6	44.8	44.7	67.4	71.2
T, K	1463	1463	1570	1570	1523	1523	1426	1426	1426	1570	1570
Element											
Li	0.253	0.275	0.243	0.257±0.020	0.247±0.014	0.218±0.011	0.210±0.014	0.243±0.012	0.226	0.160	0.138
Be	0.409±0.091	0.355±0.053	0.559	0.576±0.075	0.478±0.161	0.339±0.028	0.216±0.070	0.172±0.064	0.272±0.089	0.368±0.021	0.342±0.112
B	0.156±0.095	0.142±0.018	0.057	*0.273±0.139*	0.096±0.033	0.128±0.023	*0.898±0.237*	0.197±0.035	0.168±0.047	0.228±0.015	0.101±0.020
F	*0.331±0.076*	1.411±0.201	0.484±0.124	0.505±0.142	0.844±0.396	1.520±0.397	*4.879±1.135*	0.994±0.342	1.223±0.444	0.459±0.066	2.587±0.847
Mg	0.034	0.039	0.028	0.032	0.039	0.040±0.002	0.035	0.061	0.041	0.045±0.005	0.046±0.003
P	0.146±0.028	0.081±0.014	0.079±0.014	0.065±0.024	0.072	0.096±0.022	0.161±0.028	0.168±0.032	0.088±0.009	0.100±0.041	0.429±0.419
Cl	0.447±0.131	0.672±0.114	0.622±0.209	0.427±0.175	1.042±0.368	0.757±0.151	1.575±0.359	1.247±0.566	0.915±0.166	0.452±0.050	1.404±0.460
K	0.131±0.009	0.143	0.093±0.006	0.098	0.121	0.100	0.147	0.160	0.163	0.174	0.186
Sc	<0.072	0.312±0.093	0.082±0.031	0.118±0.139	0.082±0.036	<0.172	<0.929	<0.798	0.314±0.092	1.000±0.379	1.458±0.997
Ti	0.076±0.004	0.077	0.055	0.060±0.003	0.065	0.060	0.096	0.112±	0.090	0.197	0.164±0.032
V	<0.012	<0.072	<0.022	0.010±0.023	<0.060	<0.085	0.049±0.173	<0.273	<0.142		
Cr	0.046±0.005	0.051±0.009	0.031±0.002	0.029±0.007	0.057	0.045±0.004	*0.191±0.039*	0.075±0.023	0.108±0.028	0.105±0.016	0.108±0.024
Mn	0.000	<	<0.086	<0.0946	<0.0818	0.025±0.003	0.043±0.017	0.092±0.017	<0.086	<0.0487	
Fe	0.226	0.225	0.098±0.006	0.115	0.190	0.218±0.016	0.289	0.293±0.015	0.280	1.100±0.717	0.383±0.308
Co	0.180±0.066	0.172±0.081	0.149±0.088	0.125±0.115	0.090±0.008	0.230±0.043	*1.034±0.222*	0.214±0.093	0.303±0.071	0.922±0.189	1.593±0.690
Ni	0.518±0.103	0.301±0.202	0.162±0.104	<0.123	<0.163	0.122±0.061	1.161±0.455	0.338±0.313	0.436±0.149	0.830±0.404	<1.257
Rb	0.047	0.037±0.015	0.033±0.009	0.036±0.017	0.037±0.006	0.021±0.001	<0.083	0.067±0.026	0.018±0.003	0.000	<0.623
Sr	**2.696**	**2.407**	**1.593**	**1.572**	**1.808**	**1.739**	**3.084**	3.766	3.758	**1.550**	**1.445**
Y	0.112	0.055±0.004	0.057±0.009	0.043±0.005	0.070±0.010	0.090±0.019	*0.282±0.047*	*0.116±0.014*	0.056±0.009	2.396±1.810	0.516±0.097
Zr	0.0033±0.0010	0.0037±0.0009	0.0027±0.0007	0.0013±0.0001	0.0056±0.0017	0.0029±0.0003	0.0127±0.0020	0.0126±0.0042	0.0061±0.0014	0.0089±0.0046	<0.0010
Nb	0.0238±0.0059	0.0193±0.0111	<0.0020	<0.007	0.0107±0.0049	0.0120±0.0030	0.0821±0.0255	<0.0472	0.0173±0.0065	0.0925±0.0341	<0.1311
Cs	<0.0085	<0.0486	<0.0826	<0.1026	0.0626±0.0419	0.1085±0.0684	0.1091±0.0730	<0.2432	<0.208	<0.6077	<4.237
Ba	0.487±0.050	0.296	0.208±0.040	0.226±0.011	0.249±0.045	0.213±0.012	0.604±0.041	**0.692**	0.661	0.400	0.375
La	0.237±0.012	0.219±0.015	0.197±0.032	0.217	0.176±0.011	0.197	*0.631±0.042*	*0.490±0.041*	**0.263±0.021**	0.725±0.093	1.147±0.157
Ce	0.173	0.143±0.009	0.156±0.015	0.166±0.011	0.136	0.144	*0.407*	0.233±0.022	*0.414±0.041*	1.081	1.099±0.118
Pr	0.171	0.176±0.030	0.152±0.030	0.152±0.032	0.140	0.138±0.010	*0.440*	0.282±0.052	<0.072	1.000±0.500	0.667
Nd	0.198	0.157±0.012	0.154±0.015	0.138±0.014	0.175±0.016	0.235±0.027	*0.503*	0.276±0.033	*0.307±0.040*	1.063±0.194	0.988±0.165
Sm	0.179±0.019	*0.086±0.046*	0.106±0.018	0.124±0.018	0.122±0.022	0.188±0.030	*0.433±0.078*	0.285±0.081	0.186±0.031	6.816±5.235	1.918±0.659
Eu	0.120±0.077	0.074±0.070	0.132±0.026	0.183±0.081	0.061±0.041	<0.047	*0.616±0.285*	<1.812	<3.593	0.161±0.093	0.182±0.073
Pb	0.813±0.211	0.566±0.137	0.829±0.398	0.431±0.183	0.603±0.171	0.275±0.017	*5.179±3.435*	0.901±0.252	*2.393±0.662*	0.774±0.078	0.670±0.428

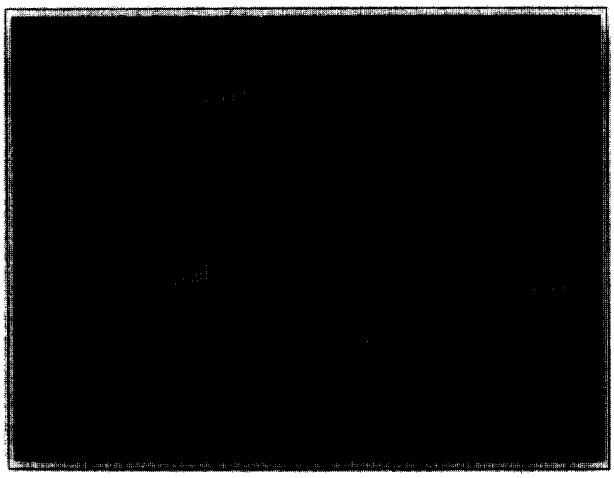

Fig. 1. Backscattered electron photographs of run 87-5 showing analysis spots in coexisting glass and plagioclase. Note the skeletal morphology of plagioclase (see text for details); ion microprobe craters (big holes) and spots left after electron microprobe analyses (smaller mounds). The ion microprobe primary beam sputters away the carbon coat around the spots, causing charging in the SEM images and leading to the bright shadows around the ion microprobe craters.

well above ion microprobe detection limit for Lu and Er (e.g., MacPherson and Davis, 1994; Simon et al., 1994). We also made an attempt to analyze Lu in plagioclase and in glass with the University of Chicago electron microprobe for run series 101 and 99. We found a highly curved background in both plagioclases. We were able to find a small peak in one sample, and no discernable peak in the other.

Because concentrations of heavy REE (HREE) in plagioclase at natural concentration levels are extremely low (less than 0.3 ppm) and we cannot analyze them with the ion microprobe, we are not considering Er and Lu further in this work. However, we note that at doped concentration levels of REE, plots of ln (D_{REE}) vs. ionic radius for the two analyzed run series 101 and 99 (An_{75} and An_{55}) show a steady drop in D_{REE} with decreasing ionic radius (Fig. 2). Similar experimental results were reported recently by Simon at al. (1994) for anorthite measured by ion microprobe on doped samples, and Phinney and Morrison (1990) for natural $\sim An_{83}$ plagioclase determined by neutron activation analysis (see Fig. 4 below).

4.2. Partition Coefficients for Different Groups of Elements

In this section we compare our measured D_t at natural concentrations with (1) the electron microprobe D_t for doped concentrations of Drake (1972), (2) other experimentally determined D_t for plagioclase of different compositions crystallized from silicate melts, and (3) a compilation of published D_t values calculated from phenocryst/matrix concentration ratios for different trace elements in volcanic rocks. The volcanic data used includes rocks varying in composition and alkalinity for which authors provide the anorthite content of plagioclase. The primary purpose of using volcanic data is to highlight the range of natural variations and compare our results with them. The comparison is done on ln (D_t) vs. X_{An} diagrams, because X_{An} is a measurable quantity in both experiments and nature (Fig. 3) that controls partitioning of trace elements. Table 2b contains partition coefficients D_t derived from ion microprobe analyses from Table 2a.

4.2.1. Lithium, potassium, and rubidium

The ln (D_t) values vary linearly with plagioclase composition (Fig. 3). The D_t of the small ionic radius element Li is almost independent of plagioclase composition, whereas ln (D_K) and ln (D_{Rb}) of larger ions exhibit a 1.5–2× increase from An_{80} to An_{40}. The three other existing experimentally determined partition coefficients for Rb in doped samples (McKay and Weill, 1977; Blundy and Wood, 1994) plot in the vicinity of the best-fit line, while phenocryst/matrix D_t values show broad variations around it. Ion microprobe measured D_t values plot in the middle of the reported volcanic values for K and Rb and in low end of the range for Li. The enormous variations in Li concentration in plagioclase from different environments has been noted previously and has no obvious explanation (Smith and Brown, 1988).

4.2.2. Strontium and barium

Strontium is found to be a strongly compatible element (ln (D_{Sr}) > 0) for the whole studied range of plagioclase composition. The larger ionic radius element Ba is found to be moderately incompatible for $An_{>40}$, but compatible for more sodic plagioclase (Fig. 3). Both ln (D_{Sr}) and ln (D_{Ba}) correlate negatively with X_{An}. Extensive literature exists for both experimental and volcanic Sr and Ba partitioning and the reader is referred to the comprehensive review of Blundy and Wood (1991). Figure 3 shows a good agreement between our data with the field of existing volcanic data, taken from their review.

4.2.3. Magnesium

Our results show very weak compositional dependence of Mg partitioning on plagioclase composition. This is in good agreement with the experimental results of Longhi et al. (1976), who found no compositional dependence for synthetic basalts. Experimental results of Sato (1989) plot in the proximity of our approximation line. However, partitioning of Mg, a major element in natural silicate melts, may be expected to be complex and sensitive to a number of parameters, including melt composition, temperature, and pressure, as well as possible splitting of Mg between M and T-sites in the plagioclase structure (Peters et al., 1995; for a review, see Smith and Brown, 1988, pp. 303, 310–327).

4.2.4. Iron

Since the experiments of Drake and Weill (1975) were done in air, nearly all of the Fe in the melt and plagioclase is present in the form of Fe^{3+} (e.g., Sato, 1989; Phinney, 1992). Our results show a steep increase in ln (D_{Fe}) with decreasing X_{An}. A much smoother and shallower increase exists for the other experimental (Longhi et al., 1976; Lindstrom, 1976; Phinney, 1992) and volcanic data, in which Fe is less oxidized. Partitioning of Fe is complicated because of its sensitivity to oxygen

Table 3. a- Ion microprobe-reanalyzed average concentrations of Sr, Ba, REEs and Y in coexisting glass and plagioclase for REE-doped run products (see Table 1 for experimental conditions); b- partition coefficients for these runs.

a

GLASS

Sample	99-5	101-4	101-7	99-7	99-2	101-3
n	2	2	3	2	2	2
Element ppm						
Sr	423	366	385	391	386	380
Ba	364	323	335	341	367	372
Y	**5910**	**5570**	23.7	26.9	20.0	24.2
La	**9944**	**7675**	11.8	13.2	9.6	10.4
Ce	**5015**	**11680**	29.3±0.6	38.4	21.1	24.5
Pr	3.5±0.2	3.6±0.2	4.1±0.3	4.9	3.3±0.3	3.6
Nd	10.4	10.7±0.6	**7281**	**4846**		
Sm	5.8±0.2	7.7±0.3	3.3±0.6	6.2±0.7	**20279**	**26798**
Eu	7.4	14.0	2.6±0.3	2.6±0.3	**95081**	**14260**
Gd					**10023**	**15314**
Dy			**4662**	**11197**		
Er			**4657**	**15111**		
Lu	**4997**	**13785**				

PLAGIOCLASE

Sample	99-5	101-4	101-7	99-7	99-2	101-3
An, %	**52.5**	**75.5**	**75.0**	**53.0**	**53.0**	**75.0**
n	2	2	3	2	2	2
Element ppm						
Sr	1111	550	647	1111	1098	614
Ba	147	59	71	144	185	75
Y	**140**	**126**	0.59±0.08	1.30±0.20	0.49±0.08	0.75±0.06
La	**2192**	**1079**	1.9±0.1	3.7±0.2	2.2±0.1	1.6
Ce	**687**	**1110**	2.8±0.2	6.4±0.5	2.8±0.2	2.4±0.1
Pr	0.43±0.07	0.23±0.04	0.50±0.10	0.90±0.21	0.50±0.11	0.48±0.06
Nd	1.7±0.2	0.8±0.1	**661**	**600**		
Sm	0.6±0.1	0.6±0.1			**1268**	**1686**
Eu	0.54±0.07	0.87±0.05	0.09±0.08	0.40±0.20	**637**	**984**
Gd					**463**	**769**
Dy			**137**	**352**		
Er			**84**	**293**		
Lu	**34**	**128**				

b

PARTITION COEFFICIENTS

Run	99-5	101-4	101-7	99-7	99-2	101-3
Element						
Sr	2.628	1.504	1.680	2.765	2.845	1.613
Ba	0.403	0.183	0.211	0.443	0.504	0.200
Y	**0.024**	**0.023**	0.025	0.027	0.024±0.004	0.031±0.002
La	**0.220**	**0.141**	0.163	0.258	0.229±0.013	0.155
Ce	**0.137**	**0.095**	0.095±0.007	0.166	0.134±0.011	0.097±0.005
Pr	0.124±0.022	0.063±0.013	**0.116±0.024**	**0.098±0.020**	0.142±0.034	0.132±0.019
Nd	0.168±0.025	0.074±0.013	0.091±0.001	0.121		
Sm	0.106±0.019	0.077±0.011			**0.063**	**0.063**
Eu	0.073±0.010	0.062±0.004		0.094	**0.067**	**0.069**
Gd					**0.046**	**0.050**
Dy			**0.0293**	**0.0314**		
Er			**0.0180**	**0.0194**		
Lu	**0.0069**	**0.0093**				

±1σ is given when it is larger than 5% of the value); bold script denotes doped elements.

fugacity and intramineral partitioning between the M and T sites (Smith and Brown, 1988). Sato (1989) demonstrated a 10 times increase in D_{Fe} with change of oxygen fugacity from 10–11.5 to 0.7 for a Aomposition. Losses of Fe into Pt capsules and wire loops is an additional problem in most laboratory partitioning experiments.

4.2.5. Titanium and chromium

Figure 3 indicates that the ion microprobe measured D_c values for these transition metals increase with decreasing An content. The experimental data of Lindstrom (1976) for Ti in plagioclase in doped synthetic basalts, plot below our data.

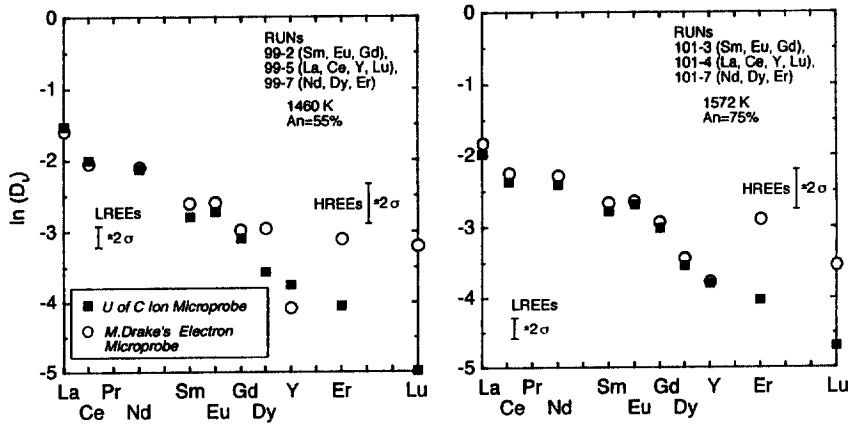

Fig. 2. Ion microprobe and electron microprobe comparison of partition coefficients for REE and Y in run series 99 and 101 of Drake (1972). Open circles are D_i from Drake and Weill (1975) electron microprobe measurements, filled squares are result of reanalyses of these run products, done in this study using the University of Chicago ion microprobe. The 2σ error bars shown are for electron microprobe analyses from Drake (1972). Ion microprobe uncertainties for these doped concentrations are less than symbol size.

Volcanic phenocryst/matrix D_i values group around our data with significant scatter.

4.2.6. *Cobalt and scandium*

The measurements of Co and Sc in plagioclase involve large corrections for molecular ions, so they should not be considered as reliable as other elements. Scandium is interfered with by SiO^+. We calculate SiO^+ from mass 46, after correcting for Ti^+ and Ca^+. We sometimes used mass 44 to calculate SiO^+, after correcting for Ca^+. The two methods give slightly different corrections and in both cases the correction amounts to 90% of the total counts at mass 45. The major interference for Co is CaO^+, which is calculated from CaO^+ at mass 56, after correction for Fe^+, $AlSi^+$, and Si_2^+. This correction is well determined, but the interference accounts for more than half of the counts at mass 59. Since the corrections for Sc and Co are so large, the reader should consider data for these elements as semiquantitative. The experimental data of Lindstrom (1976) for Sc and Co plot below our data. Volcanic phenocryst/matrix D_i values group around our data with significant scatter for cobalt . Ion microprobe-measured ln (D_{Sc}) seems to be higher than the majority of the volcanic data and may be related to large analytical uncertainty of our measurements for this element.

4.2.7. *Niobium*

The concentration of Nb in plagioclase is usually close to our ion microprobe detection limit, which accounts for the large uncertainty in partition coefficients. D_{Nb} values show a steep increase with decreasing An content. A few existing volcanic phenocryst/matrix D_{Nb} values group around our correlation line. More abundant literature data on the phenocryst/matrix D_{Ta} also plot around our correlation line (Ta has similar crystal chemical properties to Nb).

4.2.8. *Phosphorus and zirconium*

ln (D_P) and ln (D_{Zr}) exhibit the strongest negative correlations with X_{An}. The only other experimental point for ln (D_{Zr}), at An_{97} (Simon et al., 1994), plots close to our correlation line. However, most of the volcanic data for Zr, as well as for Hf, which is identical in charge and ionic radius to Zr, plot above our correlation line, especially for sodic plagioclases. It is tempting to propose that this is related to incorporation of microinclusions of zircon into plagioclase. Existing volcanic data for D_P show tremendous scatter (not shown), which is likely to be due to the presence of microscopic inclusions of apatite within plagioclase and also secondary hydrothermal alteration.

4.2.9. *Beryllium*

ln (D_{Be}) exhibits a strong positive correlation with X_{An}, the strongest among studied trace elements. $^9Be^+$ has a potential isobaric interference from $^{27}Al^{3+}$ at the low mass resolution at which the ion microprobe analyses were done. However, we note that there is no correlation between Al and Be concentrations among plagioclase of An_{40}-An_{80} and there is a negative correlation between Al and Be in the glass. The latter correlation probably reflects mixing of natural basaltic andesite glass with varying amounts of synthetic albite and anorthite used to make the starting compositions for the runs. Only a few volcanic data exist for the studied compositional range; most of the ln (D_{Be}) are for albite-rich plagioclases that plot high above our correlation curve.

4.2.10. *Boron*

ln (D_B) shows strong increase with decrease of An content, in agreement with the variations detected in volcanic data.

4.2.11. *Fluorine and chlorine*

Fluorine and chlorine, volatile elements in most magmas, also exhibit an increase in ln (D_F) and ln (D_{Cl}) with decreas-

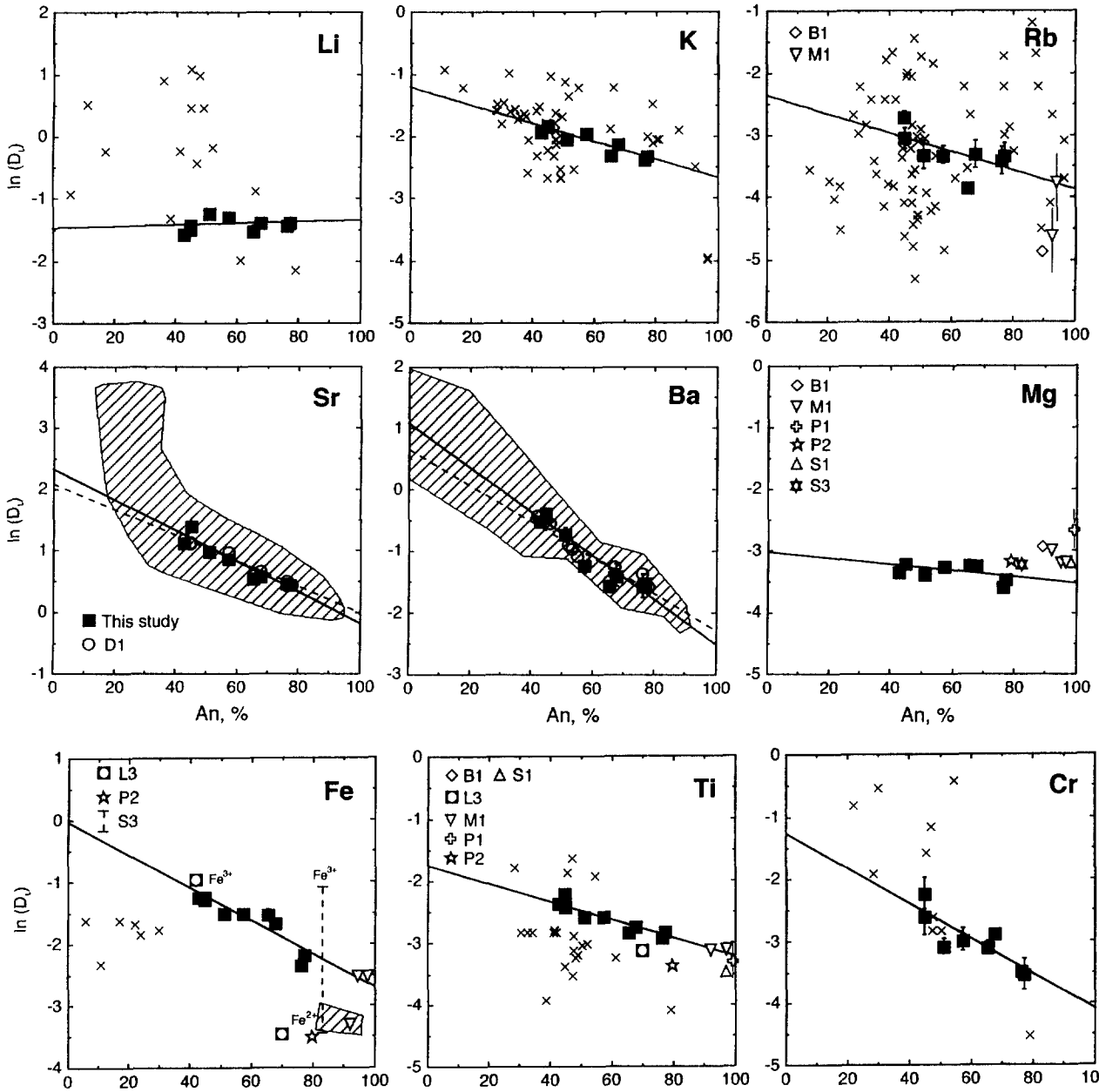

Fig. 3. Partition coefficients of trace elements as a function of An content of plagioclase. Filled squares with solid correlation lines and error bars ($\pm 1\sigma$) are our ion microprobe-measured partition coefficients at natural concentration levels of trace elements. Empty circles connected by dashed correlation lines are electron-microprobe measured D_i for the equivalent samples doped with ~1wt% of one to three different trace elements (see Drake and Weill, 1975). Empty symbols are published experimental partition coefficients for other doped experiments; Xs are existing phenocryst/matrix partition coefficients. Letter abbreviations on the legend are a shorthand for the source article and are listed beside the reference in the References section. Empty squares, and the dashed line on Y diagram are ion microprobe reanalyses of Y-doped runs (see text for discussion). Ruled areas for Fe reflect variations of $D_{Fe^{2+}}$ from experiments of Longi et al. (1976), dashed line for An_{83} reflects range in D_{Fe} as a function of oxygen fugacity in 1 atm experiments of Sato (1989); ruled areas for Sr and Ba represent phenocryst/matrix D_i from the review of Blundy and Wood (1991); for F, the ruled area represents phenocryst/matrix data from ongonites (Li-F-rich granites) of Kovalenko et al. (1984). Areas of Hf and Ta phenocryst/matrix partition coefficients are shown on the Zr and Nb diagrams, respectively.

ing An content. Some natural partition coefficients for F fit our correlation line nicely. However, a specific Li and F-rich group of granites, ongonites (Kovalenko et al., 1984; see Fig. 3 ruled area), plot significantly lower than the correlation line. Chlorine partition coefficients exhibit large uncertainty and scatter around our correlation line. Volcanic phenocrysts/matrix data show tremendous scatter (not shown), which is likely to be the result of the large volatility of Cl and the susceptibility of glass to alteration.

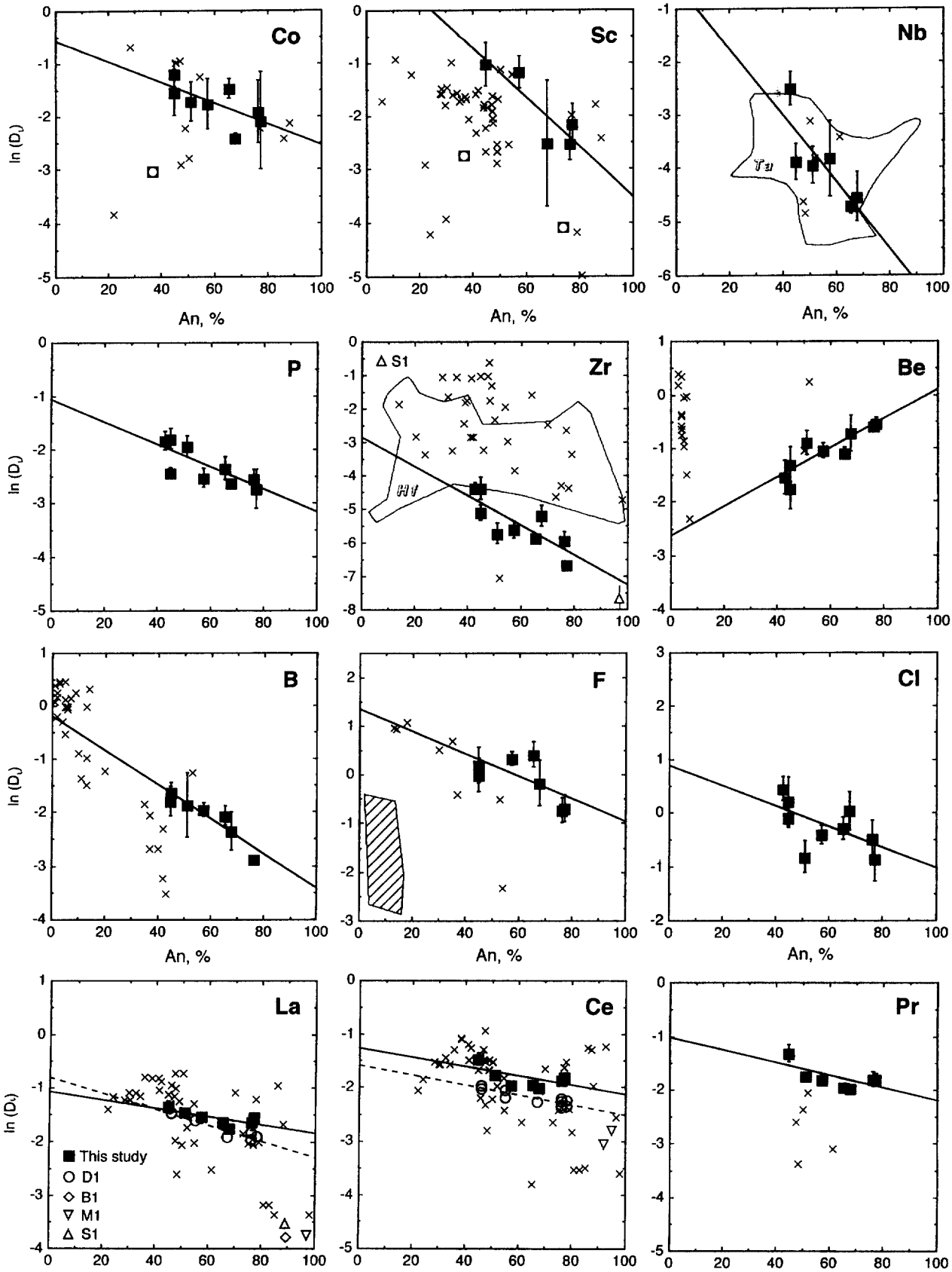

Fig. 3. (Continued)

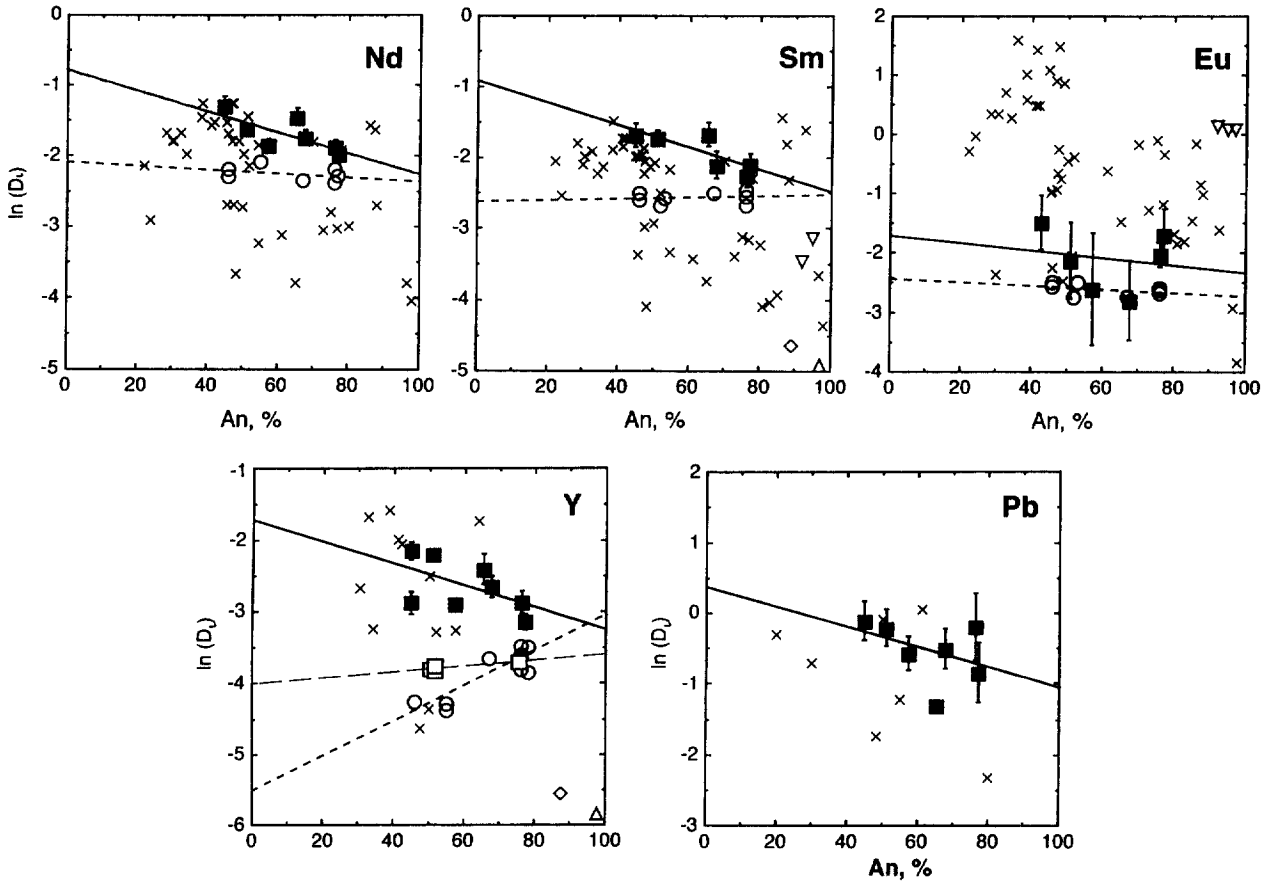

Fig. 3. (Continued)

4.2.12. Rare Earth Elements and yttrium

Several experimental studies have been done on REE and Y partitioning between plagioclase and silicate liquid (Drake, 1972; Drake and Weill, 1975; Weill and McKay, 1976; McKay and Weill, 1977; Blundy and Wood, 1994; Simon et al., 1994; Jones, 1995); in addition, many volcanic phenocryst/matrix D_i have been reported. Our work adds to this database by providing ion microprobe-measured partition coefficients at natural concentration levels. The LREE and Eu can be determined by the ion microprobe at undoped concentration levels, whereas the concentration of HREE in plagioclase are below ion microprobe detection limits. We have measured the partition coefficient of Y, which has an ionic radius intermediate between Dy and Ho and behaves like a HREE. Partition coefficients of all measured REE and Y exhibit increase with decrease of X_{An}. This result is in a general agreement with the more scattered phenocryst/matrix data (Fig. 3). The D_i values from doped experiments of Drake (1972) and other experimental results for doped samples plot below our correlation line. The next section addresses the question of comparison between doped and undoped D_i.

D_{Eu} behaves similarly to its neighboring D_{Sm} and D_{Gd}, indicating that in open air experiments Eu was almost entirely trivalent. Volcanic D_{Eu} values plot higher, because under typical natural conditions Eu is predominantly divalent. Eu^{2+} is more compatible than Eu^{3+}, as it is in experiments with $f_{O_2} < 10^{-7}$ (Drake, 1972, 1975; Weill and Drake, 1973; McKay and Weill, 1977).

4.2.13. Lead

Our data show a negative correlation between ln (D_{Pb}) and X_{An}. No other experimental data have been reported for Pb. Limited phenocryst/matrix data show that D_{Pb} increases from 0.1–0.3 for calcic plagioclase to 0.4–0.7 for sodic plagioclase (Leeman, 1979, Appendix 2).

4.2.14. Other elements

The concentrations of V, Mn, Ni, and Cs in plagioclase are below the ion microprobe detection limits (Table 2a). Upper limits for D_i can be assessed, using the analytical uncertainty of these elements in plagioclase and their concentrations in glass (see Table 2b).

4.3. Partition Coefficients of Strontium, Barium, Yttrium, and Rare Earth Elements at Natural Concentration Levels Versus Those in Doped Experiments

Figure 3 compares our ion microprobe-measured D_i with those of Drake (1972) (see Drake and Weill, 1975) for the

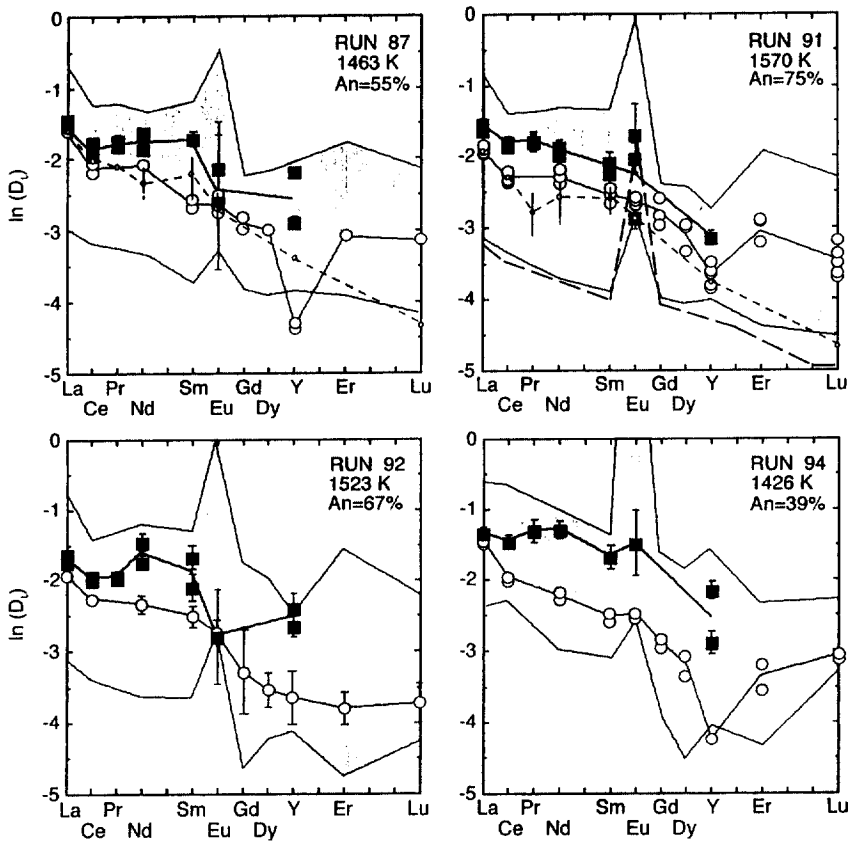

Fig. 4. REE and Y partition coefficient patterns. Squares are our ion microprobe-measured partition coefficients at natural concentration levels of trace elements (~0.3–3ppm); circles are electron microprobe-measured partition coefficients for doped runs (~1wt%); the shaded areas are existing phenocryst/matrix partition coefficients for the given plagioclase composition (± 5 mole % An). Error bars, shown for doped run 92 are ± 2σ electron probe counting precision from Drake (1972); similar errors are expected for other doped runs. The small-dashed lines shown on runs 87 and 91 are ion microprobe-measured partition coefficients for La-Ce-Y-Lu doped series (See Fig.2 and Table 3). Note that not only are partition coefficients of doped La, Ce, Y, and Lu lower than at natural concentration levels, but also Sm and Eu in these runs are lower. The wide-dashed line represents recent Phinney and Morrison (1990) phenocrysts/matrix D_t data for An_{83}.

equivalent runs, i.e., for the same temperature, X_{An}, and composition of the glass but with a different doped element.

Ion microprobe-measured D_{Sr} and D_{Ba} values overlap within analytical uncertainty with D_{Sr} and D_{Ba} values for doped concentrations (see Fig. 3 and Tables 2 and 3). Because most of our ion microprobe measurements were made on Sr-doped series (see Table 1), we could make a direct comparison for Sr in undoped runs in which REE, Y, and Ba (see Table 1) served as dopants. For these runs no difference with the equivalent Sr-doped runs was detected. They overlap with the best fit parameters of Blundy and Wood (1991), who used both volcanic and experimental partitioning of Sr and Ba.

Ion microprobe-measured D_{La} in samples doped with Sr and Ba, but not with REE, agree with electron microprobe values from REE-doped samples. Ion microprobe-measured D_t values for Ce, Pr, and Eu exhibit concave upward slopes, in contrast to the linear relationship between ln (D_t) and An content for the electron microprobe-determined values. Within analytical error, a convincing case cannot be made for a difference between ion and electron microprobe measurements on Eu-undoped and Eu-doped samples, respectively. However, the best fit lines to the ion microprobe-measured D_t values for Ce, Nd, Sm, and Y in samples doped with Sr or Ba, but not with REE, are systematically higher than those obtained from electron microprobe values from REE-doped samples and, for Nd, Sm, and Y, exhibit significantly different slopes. Note that partition coefficients obtained from doped samples reported in the literature (Weill and McKay, 1976; Blundy and Wood, 1994; Simon et al., 1994; McKay, 1995 cit. after Jones, 1995) for more Ca-rich plagioclase are smaller than the values that would be extrapolated from the present work.

By plotting ln (D_t) of REE and Y vs. their atomic number (concordant with the small incremental ionic radius decrease) one can expect to observe a smooth curve (Fig. 4; see also Fig.2). This graph allows a check of both ion microprobe measured and electron microprobe measured D_t values for mutual consistency and compares all D_t on the same graph. Both doped D_t and natural concentration D_t values exhibit a progressive decrease with increasing atomic number. The smoothness of this curve for doped concentrations on the graph makes us confident about the mutual consistency of electron-microprobe data for different REE and Y.

The ion microprobe-measured D_t values at ppm levels also form a relatively smooth curve (except LREE of run 92),

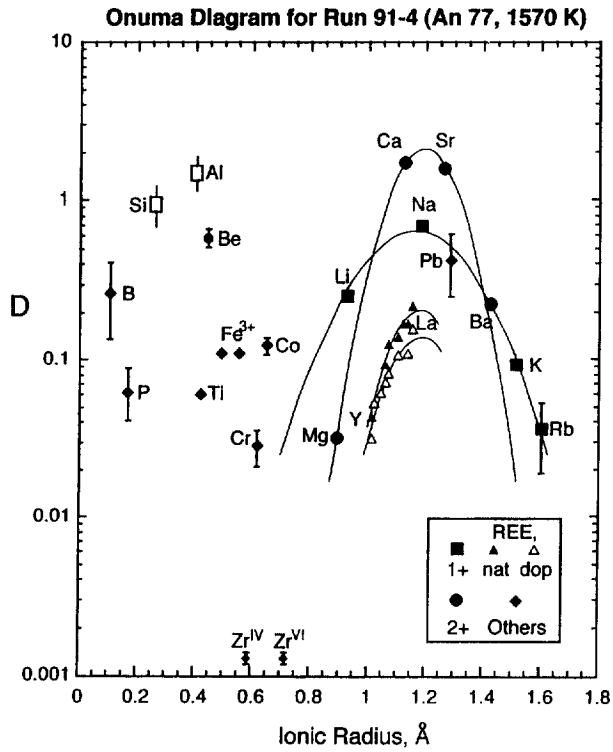

Fig. 5. Onuma diagram for the partition coefficients of the studied trace elements (see Table 2b). Parabolas are drawn through the element of the same valence group. Ionic radii are from Shannon (1976), probable coordination numbers of ions in the feldspar structure are taken from Smith and Brown (1988) and for Zr both likely numbers are shown in superscript in roman numerals.

repeating the details of the shape of electron microprobe curve for doped samples for the same compositions and temperatures. However, the ppm-based D_t values are always higher than the wt%-level D_t ones, more so for heavier REE and Y. This difference cannot be explained by plagioclase contamination by the glass or by ion microprobe interferences.

4.4. Partition Coefficients Versus Ionic Radii

An Onuma diagram (Onuma et al., 1968) relates ionic radius of a substituting ion to the logarithm of its D_t value (Fig. 5). When several elements of the same group are plotted vs. their ionic radii, the result is a symmetric inverted parabolic curve with a maximum at the size of the ionic site of the preferred substitution. The location of the maxima on similar curves for other groups of elements indicates the ionic site in which substitution occurs (Philpotts, 1978). The Onuma diagram allows a check of D_t values of different elements for mutual consistency. Interpolation and extrapolation of the parabolic curve to the size of an ion of interest can be used to predict its D_t value.

Alkali, alkaline earth, and REE reported in this study obey the Onuma-type relationship (e.g., Fig. 5) and form three different parabolas with maxima corresponding to the size of VIII-fold coordinated M-site in plagioclase, occupied by Ca^{2+} and Na^{+}. It is thus probable that all these elements partition into M-site. We obtained an especially good parabolic fit for alkalies and alkaline earths in every run with $r^2 > 0.99$. Log D of REE at both natural and at doped concentration levels can also be nicely fit with a segment of a parabola ($r^2 = 0.95$), in which maxima are coincident with the size of the M-site. However, REE and Y partition coefficients at natural concentration levels plot higher than that at doped concentrations, forming two closely enclosed parabola in each run (see Fig. 5) with the former above the latter. This result is an obvious replication of the Fig. 4, showing higher D_{REE} and D_Y at natural concentration levels.

Other published phenocryst/matrix D_t as well as other experimentally determined D_t values for doped samples behave in a similar fashion (Onuma et al., 1968; Philpotts, 1978; Moeller, 1988; Blundy and Wood, 1994).

The partition coefficient of Pb plots in the vicinity of one of these parabolas which may also indicate its substitution into M site. Most of the small ions (Fe^{3+}, Ti^{4+}, P^{5+}, B^{3+}, and Be^{2+}) plot well off to the left of the M site, closer to the size of IV-coordinated T-site, occupied by Al^{3+} and Si^{4+}. This suggests that their substitution, if it is structural, may be into the tetrahedral site (e.g., Fleet, 1992; Smith and Brown, 1988). Magnesium, which plots on the left downslope of parabola, was shown to partly partition into T-site as well (Peters et al., 1995). The transition metals Cr and Co, as well as Zr and Nb, have very low D_t values and plot in between the M-site parabola and T-site. The nature of the substitution of these elements is unclear and may be nonstructural, defect related (Smith and Brown, 1988).

4.5. RT ln (D_t) Versus X_{An} and ln (D_t) vs. X_{An}

We showed in Fig. 3 that ln (D_t) is well a linear function of the following form for almost every element studied:

$$ln\ (D_t) = a^* X_{An} + b^*. \quad (1)$$

Considering the parameter RT ln (D_t) instead of ln (D_t), we

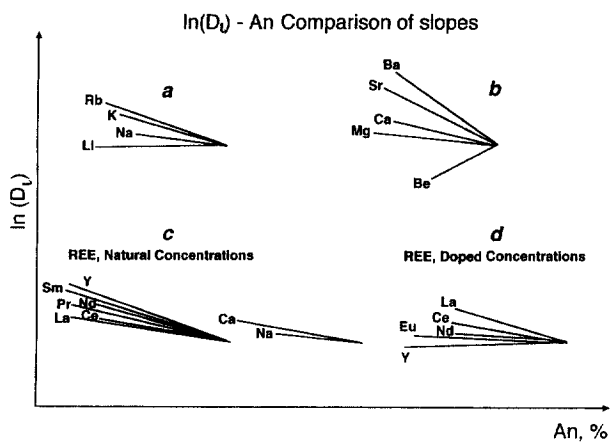

Fig. 6. The slope comparison for partition coefficients on ln (D_t) vs. X_{An} graphs (see Fig. 3) for (a) alkali elements, (b) alkaline earth elements, (c) REE at natural concentration levels (~1ppm), and (d) REE at doped concentration levels (1 wt%). Note that in cases (a), (b), and (d) slope magnitude increases from positive for smaller ions, to negative for larger ones and the magnitude of the slope increases with the increase of ionic radius. In case (c) we observe the opposite trend.

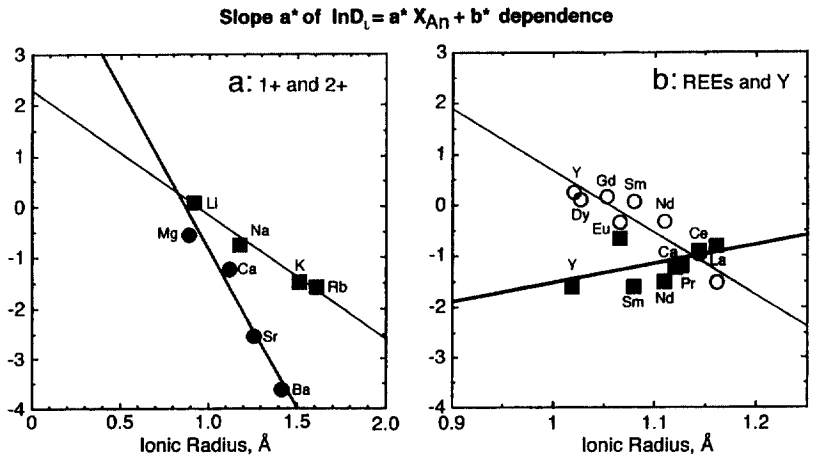

Fig. 7. The slope a* (in the relation ln (D_i) = a* X_{An} + b* for $0 < X_{An} < 1$) vs. VIII-coordinated ionic radius for (a) alkali elements (squares) and alkaline earth elements (circles), (b) trivalent REE at natural concentration levels (squares), and REE at doped concentration levels (open circles).

account for the polythermality of melts at different X_{An}. Use of RT ln (D_i) rather than ln (D_i) expresses the energetic significance of partition coefficients. By plotting RT ln (D_i) vs. X_{An} we find that RT ln (D_i) is also linearly dependent on X_{An}:

$$RT\ ln\ (D_i) = a\ X_{An} + b \qquad (2)$$

where R is the gas constant. This is a result of the linear dependence of plagioclase composition on temperature in our experiments, as more An-rich plagioclase crystallizes at higher temperatures. The relationship between temperature and plagioclase composition is best described as

$$1/T = m\ X_{An} + n, \qquad (3)$$

where $m = -2.04 \times 10^{-4}$ and $n = 7.92 \times 10^{-4}$ for the compositional range $0.4 < X_{An} < 0.8$, $r^2 = 0.985$.

The character of the compositional dependence of RT ln (D_i) for various elements replicates all major features of ln (D_i)-X_{An} dependence, but is expressed in energy units. As is the case for the ln (D_i)- X_{An} relationship, for most elements the slope a is negative, indicating that D_i values are normally higher for albite-rich compositions. The magnitude of the increase is different for different elements in the studied plagioclase compositional range (An_{40-80}) and varies from 0 to 4.

Blundy and Wood (1991, Eqn. 10) have shown for Sr that the RT ln (D_{Sr}) dependence can be expressed as a linear function of X_{An} within the accuracy of the fit:

$$RT\ ln\ (D_{Sr}) = -\Delta H_i^\circ - T\Delta S_i^\circ - W_{SrAb} + (W_{SrAb} - W_{SrAn} + W_{AbAn})\,X_{An}, \qquad (4)$$

where Ws are regular solution model parameters of interaction in corresponding binaries, and ΔH_i° and ΔS_i° are standard enthalpies and entropies of fusion. This linearity is explained by the fact that nonideality in Sr-Ab join is much larger than in Ab-An join, and W_{AbAn} is smaller than both W_{SrAb} and W_{SrAn}. Other trace elements, whose sizes deviate more than Sr from that of M-site are expected to exhibit similar relationships.

Equations 2 and 4 include both compositional and temperature influences on partition coefficients. In the experiments considered in this paper, temperature variations between different runs did not exceed 144° and are in the high-temperature interval (see Table 1). At high magmatic temperatures, a 150 degree decrease produces less than 10% variations in the RT ln (D_i) parameter (see Eqn.2), which is often within analytical error of the D_i determination. Blundy and Wood (1991) demonstrated for Sr that even for larger variations in temperatures, the compositional dependence, X_{An}, is the dominant factor.

Table 4 gives the slope a and the intercept b with uncertainties, which were determined using the method of Williamson (1968) for weighted linear regression. This method weights data points by the magnitudes of the uncertainties.

4.6. Compositional Dependence of Partition Coefficients for Different Groups of Elements

Plagioclase/melt partition coefficients show a linear dependence on plagioclase composition that is described by Eqns. 1 and 2. The Onuma diagram shows the variation of D_i values for a fixed plagioclase composition. Here we illustrate that not only does the magnitude of D_i change with ionic radius, but also its plagioclase compositional dependence changes.

Let us consider the slope parameter a* on Fig. 3. In Fig. 6, we copied the following slopes from Fig. 3: ion microprobe-measured ln (D_i) for the alkalies, alkaline earths, and undoped REE and Y and electron microprobe-measured ln (D_i) for doped REE and Y. By plotting these slopes on the same scale we find a systematic increase of slope with increasing atomic number for the elements of the same valence. If the slopes for Ca^{2+} and Na^{+}, major cations substituting into the M-site, are taken as references, we find that cations smaller in ionic radius than Ca^{2+} or Na^{+} exhibit a flatter slope, while larger ions show steeper slope. The smallest ions of the each group (Li^{+}, Be^{2+}, and Y^{3+}) even exhibit a positive slope. In contrast to results for ln (D_{REE}) for doped samples, ln (D_{REE}) for LREE and Y at natural concentration levels display only a limited slope change, and it seems to increase from La to Y, or with decrease of REE

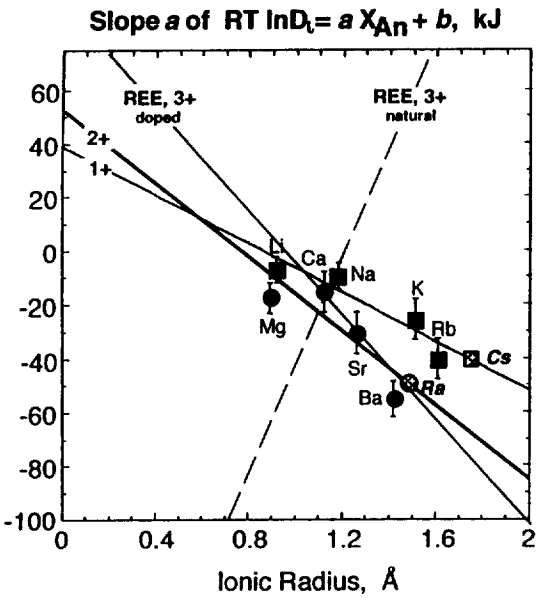

Fig. 8. The slope a (in the relation RT ln (D_t) = a X_{An} + b for 0 < X_{An} < 1) for different valence groups of elements vs. VIII-coordinated ionic radius, along with extrapolated values for Cs and Ra. The use of Onuma diagrams provides an intercept b so that partition coefficients can be predicted for Cs and Ra: RT ln (D_{Cs}) = −41(±10) X_{An} − 57(±10) and RT ln (D_{Ra}) = −49(±10)X_{An} − 5(± 1). Uncertainties include the possibility of either VIII- or IX-coordinated ionic radii, both possible for larger ions in plagioclase structure (Smith and Brown, 1988).

ionic radius. This behavior is just the opposite of that for other elements and results for REE at doped levels.

By plotting the magnitude of slope a* vs. ionic radius (Fig. 7), we find a linear correlation. The slope of a* dependence from ionic radius is the steepest for REE at doped concentrations, medium for alkali earths, and the flattest for alkalies. However, the data (see Fig. 7b) for natural level REE and Y do not obey the common rule of increasing slopes with increasing valence. Perhaps a significant portion of REE and Y at natural concentration level (see discussion in section 4.3 and below) partitions into sites whose sizes and elastic properties are not similar to the M-site. In addition, the dependence of slope on ionic radius is not observed for smaller elements (e.g., P^{5+}, Zr^{4+}, Nb^{5+}, Ti^{4+}) which do not partition into the M site.

Figure 8 shows a similar relationship for the slope a in the RT ln (D_t) vs. X_{An} dependence. The linear character of this dependence allows extrapolation of the line to the ionic radius of an element of interest (for example, Cs or Ra) and prediction of the slope a of their compositional dependence in Eqn. 2. Similarly to the dependence Eqn. 1, the RT ln (D_t) vs. X_{An} compositional dependence is the weakest for ions smaller than the size of M site: Li^+, Mg^{2+}, $HREE^{3+}$, and Y^{3+}. These ions exhibit very weak positive or almost no dependence of RT ln (D_t) on X_{An}. RT ln (D_t) of the larger ions Rb^+, Ba^{2+}, and La^{3+} exhibits the strongest negative slope with X_{An} and, these ions are, therefore, the most sensitive to plagioclase compositional change. Figure 8 also demonstrates that this increase in slope is the largest for doped REE^{3+}, intermediate for alkaline earths, and the weakest for alkalies. The observed variations in the slope vs. ionic radii and valence group clearly demonstrate the importance of crystal chemical control of ions substituting into M-site.

5. DISCUSSION

5.1. Discrepancy between REE Partition Coefficients in Doped versus Natural Concentration Levels

Why is there a discrepancy between natural and doped partition coefficients of REE and Y, but no such discrepancy for Sr and Ba, and possibly La? For La, however, the discrepancy exists in slope of the regression line (see Figs. 3 and 6). It should be pointed out that the concentrations of Sr and Ba at natural concentration levels in plagioclase (>100 ppm) are more than one order of magnitude higher than the concentrations of REE (0.3–3 ppm). We also showed above (see Figs. 3 and 4) that the discrepancy is larger for heavier REE and Y, whose concentrations are ~2 times smaller than for LREE. This raises the possibility that higher D_t values at the ~1 ppm concentration level in plagioclase are due to a change in substitution mechanism at low concentration.

One possibility for the discrepancy is that at the natural ~1 ppm level of concentration of heterovalent REE a certain portion of them may reside in defect sites. At doped REE concentration levels, all defect sites are saturated, and the relative importance of the defect site substitution vanishes. Substitution at doped concentration is, therefore, largely structurally controlled.

The origin of defect sites may be due to several factors. Fast crystallization of plagioclase in the experimental runs, as well as in many volcanic plagioclases, may cause the appearance of defect sites. The order-disorder state of feldspar is another important factor controlling the concentration of the defect sites. Disordered feldspars show greater ability to accommodate foreign atoms, as is demonstrated for the most abundant trace element in plagioclase, Fe (Petrov et al., 1989b). In addition, as opposed to homovalent substitution of Sr and Ba and alkalies into the M-site, the heterovalent substitution of REE^{3+} and Y^{3+} into this site requires a monovalent ion or an electron defect center (e.g., Petrov et al., 1989a) to compensate for the charge excess. The doping with REE can by itself cause the appearance of the defect sites. D'Arco and Piriou (1989) presented fluorescence spectra for Eu^{3+} in the synthetic polycrystalline anorthite and demonstrated that substitution of Eu^{3+} for Ca^{2+} is accompanied by the strong deformation of the network and the appearance of defect sites. Kimata (1988) demonstrated that the Eu anorthite endmember is strongly nonstoichiometric and the crystal structure can tolerate up to 8% empty sites in the europium position. Obviously, this could be the case for other REE, which have similar ionic radii.

Arguing against defect site substitution is the regular behavior on the Onuma diagram (Fig. 5) of REE partition coefficients obtained from both doped and undoped samples. This regular behavior strongly suggests substitution of the REE into the M-site in both doped and undoped experiments. Such structural substitution might also be expected because the samples which were not doped with REE were doped with Sr or Ba. These ions are expected to compete for the same defect sites as the REE, and should effectively swamp any defect site availability. It

Table 4. Least square approximation parameters for RT ln (D_i) = a X_{An})+b dependence, kJ.

This study, natural concentration levels, ion microprobe					Drake (1972), doped concentration levels, electron microprobe		
Element	a	$\pm a$	b	$\pm b$	**Element**	a	b
Li	-6.9	1.9	-12.1	1.0	**La**	-25.4	-5.5
Be	28.2	6.1	-29.5	4.1	**Ce**	-20.2	-14.3
B	-0.61	0.5	9.9	3.8	**Nd**	-12.8	-19.9
F	-37.8	11.5	23.6	7.1	**Sm**	-9.2	-26.1
Na	-9.4	1.0	2.1	0.5	**Eu**	-14.3	-23.6
Mg	-26.1	1.1	-25.7	0.7	**Gd**	-9.1	-30.4
Al	-0.3	0.8	5.7	0.4	**Dy**	-11.4	-32.4
Si	-2.0	0.2	-0.04	0.08	**Y**	14.7	-58.6
P	-30.7	4.6	-12.1	2.9	**Er**	-3.0	-38.4
Cl	-24.5	9.5	11.0	5.3	**Lu**	-31.1	-22.1
K	-25.5	1.2	-10.2	0.7	**Sr**	-18.9	21.5
Ca	-15.2	0.6	17.9	0.3	**Ba**	-32.0	7.4
Sc	-94.2	28.3	37.4	18.4	**Sm/Nd**	3.6	-6.3
Ti	-28.9	1.5	-15.4	1.0			
Cr	-44.0	6.3	-9.3	4.1			
Fe	-35.2	1.9	4.5	1.1			
Co	-59.9	10.8	12.2	7.0			
Rb	-40.0	6.7	-15.1	3.8			
Sr	-30.4	1.1	28.5	0.7			
Zr	-90.4	5.5	-15.3	3.6			
Ba	-55.0	2.4	19.1	1.3			
Y	-48.1	3.7	-3.4	1.9			
La	-10.8	2.6	-12.4	1.8			
Ce	-17.5	2.3	-12.4	1.4			
Pr	-22.5	4.1	-9.3	2.7			
Nd	-19.9	3.6	-9.4	2.0			
Sm	-25.7	6.3	-7.7	3.9			
Eu	-16.1	16.1	-14.2	11.3			
Pb	-60.5	11.8	25.3	7.8			
K/Rb	14.5	5.5	4.9	3.1			
Rb/Sr	-9.6	5.5	43.6	3.2			
Sm/Nd	-5.8	2.0	1.6	1.9			

Approximation parameters a, $\pm a$, b, $\pm b$ were determined using Williamson (1968) routine.

should also be noted that the only credible reports of defect site substitution at sub-ppm concentrations, the work of Harrison and Wood (1980), on high purity compositions has subsequently been shown to be an analytical artifact by Beattie (1993).

That Sr, Ba (and, possibly La) show the same partition coefficient in both REE-doped and undoped experiments precludes a clear conclusion. We have shown that the results are unlikely to be analytical artifacts, but no compelling case can be made against structural substitution of the REE into the M-site in plagioclase. A possible resolution is that the Henry's law constant at doped vs. undoped levels may differ, but we have no firm evidence to that effect. It is clear that, when analytically feasible, experiments should be conducted at natural concentration levels.

5.2. Applications

The compositional dependence of D_i in the simple linear form RT ln (D_i) = a X_{An} + b has a general petrologic utility. In attempts to reconstruct the primary magma composition, based on trace element composition of the liquidus plagioclase, one almost always deals with plagioclase of different X_{An}, which has crystallized at different temperatures. This compositional diversity may be displayed by the zoning in a single crystal, or by generations of crystals of different X_{An} in a single rock or even in different magmatic bodies. The acceptance of a single-value D_i, as it was the common practice until recently, may be strongly misleading in such a reconstruction and comparison of the "reconstructed" compositions. As it is seen from Fig. 3, ln (D_i) depends strongly on X_{An}, so that the "recon-

structed'' trace elemental primary melt composition may vary by up to one order of magnitude if this dependence is ignored. Various elements of different ionic radius display different magnitudes of such a dependence. It is crucial, therefore, to understand the ''sensitivity'' of each trace element to this compositional dependence. Elements with small value of the slope parameter a are less sensitive to the composition. Not only do larger ions have smaller (and less certain) D_i, they also exhibit stronger slope of compositional dependence of D_i from X_{An} (Figs. 6–8). The resulting error of such a reconstruction should be the smallest for smaller ions, and largest for larger ions.

In natural applications, temperature, the second unknown in Eqn. 3, is a parameter which can be determined by applying different mineralogical geothermometers. The typical uncertainty of such a determination (± 50°) is within the error associated with employment of the compositional dependence of D_i, because the temperature dependence is naturally embedded into the compositional dependence of plagioclase composition (see above and Blundy and Wood, 1991).

The other important parameters are represented by distribution coefficients of element pairs, e.g., $K_{Sm/Nd}$, $K_{Rb/Sr}$, $K_{K/Rb}$, (Table 4) for geochemically important element ratios. Remarkably, $K_{Sm/Nd}$, $K_{Rb/Sr}$, and $K_{K/Rb}$ exhibit almost no or weak dependence on plagioclase composition (slope in Table 3 is close to 0). This has significance for the isotope analyses of plagioclase separates, showing that even the strongly zoned crystals will have similar $K_{Sm/Nd}$, $K_{Rb/Sr}$, $K_{K/Rb}$ D_i ratios in zones of different composition.

Acknowledgments—The work is a part of INB's Ph.D. thesis. It was supported by the National Aeronautics and Space Administration through Grants NAGW-3384 (to AMD) and NAGW 3348 (to MJD) and the National Science Foundation through grant EAR 9417787 to A. T. Anderson. We are grateful to I. M. Steele for the help with electron microprobe analyses, A. T. Anderson, L. Ya. Aranovich, and J. V. Smith for discussions, and J. D. Blundy and J. J. Papike for helpful reviews.

REFERENCES

Antipin V. S., Kovalenko V. I., and Petrov L. L. (1982) Partition of boron between phenocrysts and matrix of effusive and subvolcanic rocks. *Geokhimya* **11**, 1639–1660. **(A1)**

Beattie P. (1993) The occurrence of apparent non-Henry's law behavior in experimental partitioning studies. *Geochim. Cosmochim. Acta* **57**, 47–55.

Beckett J. R. and Grossman L. (1988) The origin of type C inclusions from carbonaceous chondrites. *Earth Planet. Sci. Lett.* **89**, 1–14.

Bindeman I. N. (1998) Trace element partitioning between plagioclase feldspar and melt: A study of experiments and application to magmatic elvolution. Ph.D. dissertation, Univ. Chicago.

Bindeman I. N., Davis A. M., and Wickham S. M. (1998) 400 Ma of mafic magmatism evolution in a single lithospheric block: an ion microprobe study of the relict plagioclase phenocrysts in mafic rocks of Transbaikalia, Russia. (in prep.)

Blundy J. D. and Shimuzu N. (1991) Trace element evidence for plagioclase recycling in calc-alkaline magmas. *Earth Planet. Sci. Lett.* **66**, 178–197.

Blundy J. D. and Wood B. J. (1991) Crystal-chemical control on the partitioning of Sr and Ba between plagioclase feldspar, silicate melts, and hydrothermal solutions. *Geochim. Cosmochim. Acta* **55**, 193–209.

Blundy J. D. and Wood B. D. (1994) Prediction of crystal-melt partition coefficients from elastic moduli. *Nature* **372**, 452–454. **(B1)**

Carmichael I. S. E. (1965) Trachytes and their feldspar phenocrysts. *Mineral. Mag.* **34**, 107–125. **(C1)**

Carmichael I. S. E. and McDonald A. (1961) The geochemistry of some natural acid glasses from the north Atlantic Tertiary volcanic province. *Geochim. Cosmochim. Acta* **25**, 189–222. **(C2)**

D'Arco P. and Piriou B. (1989) Fluorescence spectra of Eu3+ in synthetic polycrystalline anorthite: distribution of Eu^{3+} in the structure. *Amer. Mineral.* **74**, 191–199.

Davis A. M., MacPherson G. J., Clayton R. N., Mayeda T. K., Sylvester P. J., Grossman L., Hinton R. W., and Laughlin J. R. (1991) Melt solidification and late-stage evaporation of a FUN inclusion from the Vigarano CV3 chondrite. *Geochim. Cosmochim. Acta* **55**, 621–637.

Drake M. J. (1972) The distribution of major and trace elements between plagioclase feldspar and magmatic silicate liquid: an experimental study. Ph.D. dissertation, Univ. Oregon. **(D1)**

Drake M. J. (1975) The oxidation state of europium as an indicator of oxygen fugacity. *Geochim. Cosmochim. Acta* 39, 55-64.

Drake M. J. and Holloway J. R. (1978) ''Henry's Law'' behavior of Sm in a natural plagioclase/melt system: importance of experimental procedure. *Geochim. Cosmochim. Acta* **42**, 679–683.

Drake M. J. and Weill D. F. (1972) New rare earth elements standards for electron microprobe analysis. *Chem. Geol.* **10**, 179–181.

Drake M. J. and Weill D. F. (1975) Partition of Sr, Ba, Eu^{2+}, Eu^{3+}, and other REE between plagioclase feldspar and magmatic liquid: an experimental study. *Geochim. Cosmochim. Acta* **39**, 689–712.

Dudais M. J., Schmitt R. A., and Harward M. E. (1971) Trace element partitioning between volcanic plagioclase and dacitic pyroclastic matrix. *Earth Planet. Sci. Lett.* **11**, 440–446. **(D2)**

Dun T. and Sen C. (1994) Mineral/matrix partition coefficients for orthopyroxene, plagioclase, and olivine in basaltic to andesitic systems: a combined analytical and experimental study. *Geochim. Cosmochim. Acta* **58**, 717–733. **(D3)**

Ewart A. and Griffin W. L. (1994) Application of proton-microprobe data to trace element partitioning in volcanic rocks. *Chem. Geol.* **117**, 251–284. **(E1)**

Fleet M. E. (1992) Tetrahedral-site occupancies in reedmergnerite and synthetic boron albite ($NaBSi_3O_8$). *Amer. Mineral.* **77**, 76–84.

Francalanci L. (1989) Trace element partition coefficients for minerals in shoshonitic and calc-alkaline rocks from Stromboli Island (Aeolian Arc). *Neues Jahrb. Mineral.* **160**, 229–247. **(F1)**

Fujimaki H., Tatsumoto M., and Aoki K. (1984) Partition coefficients of Hf, Zr, and REE between phenocrysts and groundmasses. *J.Geophys. Res.* **89**, B662–B672 (suppl.). **(F2)**

Giletti B. J. (1994) Isotopic equilibrium/disequilibrium and diffusion kinetics in feldspars. In *Feldspar and Their Reactions* (ed. I. Parsons), pp. 351–382.

Giletti B. J. and Casserly J. E. D. (1994) Strontium diffusion in plagioclase feldspars. *Geochim. Cosmochim. Acta* **58**, 3785–3793.

Harrison W. and Wood B.J. (1980) An experimental investigation of the partitioning of REE between garnet and liquid with reference to the role of defect equilibria. *Contrib. Mineral. Petrol.* **72**, 145–155.

Higuchi H. and Nagasawa H. (1969) Partition of trace elements between rock forming minerals and host volcanic rocks. *Earth Planet. Sci. Lett.* **7**, 281–287. **(H1)**

Hinton R. W., Davis A. M., Scatena-Wachel D. E., Grossman L., and Draus R. J. (1988) A chemical and isotopic study of hibonite-rich refractory inclusions in primitive meteorites. *Geochim. Cosmochim. Acta* **52**, 2573–2598.

Hoover J. D. (1978) The distribution of samarium and thulium between plagioclase and liquid in the systems D_i-An, Ab-An-D_i at 1300°C. *Carnegie Inst. Wash. Yearb.* **77**, 703–709.

Jones J.H. (1995) Experimental trace element partitioning. In *Rock Physics and Phase Relations; A Handbook of Physical Constants, Ref. Shelf 3*, pp. 73-104. AGU.

Kimata M. (1988) The crystal structure of non-stoichiometric Eu-anorthite: an explanation of the Eu-positive anomaly. *Mineral. Mag.* **52**, 257–265.

Kovalenko V. I., Antipin V. S., and Petrov L. L. (1977) Distribution coefficients of beryllium in ongonites and some notes on its behavior in the rare metal lithium-fluorine-granites. *Geochem. Intl.* **14**, 129–141. **(K2)**

Kovalenko V. I., Antipin V. S., Kovalenko N. I., Ryabchikov I. D., and

Petrov L. L. (1984) Fluorine distribution coefficients in magmatic rocks. *Geochim. Intl.* **21**, 66–84. **(K1)**

Kravchuk I. K., Chernysheva I. V., and Urusov V. S. (1980) Element distribution between plagioclase phenocrysts and groundmass as an indicator for crystallization conditions of the basalts in the southern vent of Tolbachik. *Geochem. Intl.* **17**, 18–24. **(K3)**

Leeman W. P. (1979) Partitioning of Pb between volcanic glass and coexisting sanidine and plagioclase feldspars. *Geochim. Cosmochim. Acta* **43**, 171–175. **(L1)**

Lemarchand F., Villemant B., and Calas G. (1987) Trace element distribution coefficients in alkaline series. *Geochim. Cosmochim. Acta* **51**, 1071–1081. **(L2)**

Lindstrom D. J. (1976) Experimental study of the partitioning of the transitional metals between clinopyroxene and coexisting silicate liquids. Ph.D. dissertation, Univ. Oregon. **(L3)**

Lofgren G. E. (1974) An experimental study of plagioclase crystal morphology; isothermal crystallization. *Amer. J. Sci.* **274**, 243–273.

Longhi J., Walker D., and Hays J. F. (1976) Fe and Mg in plagioclase. *Proc. 7th. Lunar Planet. Sci. Conf.*, 1281–1300. **(L4)**

MacPherson G. J. and Davis A. M. (1993) A petrologic and ion microprobe study of a Vigarano Type B refractory inclusion: Evolution by multiple stages of alteration and melting. *Geochim. Cosmochim. Acta* **57**, 231–243.

MacPherson G. J. and Davis A. M. (1994) Refractory inclusions in the prototypical CM chondrite, Mighei. *Geochim. Cosmochim. Acta* **58**, 5599–5625.

McKay G. A. (1989) Partitioning of rare earth elements between major silicate minerals and basaltic melts. In *Reviews in Mineralogy* (ed. B. R. Lipin and G.A. McKay), Vol. 21, pp. 45–77. **(M1)**

McKay G. A. and Weill D. F. (1977) KREEP petrogenesis revisited. *Proc. 8th Lunar Planet. Sci. Conf.*, 2339–2355.

Moeller P. (1988) The dependence of partition coefficients on differences of ionic volumes in crystal-melt systems. *Contrib. Mineral. Petrol.* **99**, 62–69.

Morse S. A. (1984) Cation diffusion in plagioclase feldspar. *Science* **225**, 504–505.

Mysen B. O. (1978) Limits of solution of trace elements in minerals according to Henry's Law: review of experimental data. *Geochim. Cosmochim. Acta* **42**, 871–885.

Nagasawa H. and Schnetzler C. C. (1971) Partitioning of rare earth, alkalielements between phenocrysts and acidic igneous rocks. *Geochim. Cosmochim. Acta* **35**, 953–968. **(N1)**

Nash W. P. and Crecraft H. R. (1985) Partition coefficients for trace elements in silicic magmas. *Geochim. Cosmochim. Acta* **49**, 2309–2332. **(N2)**

Onuma N., Higuchi H., Wakita H., and Nagasawa H. (1968) Trace element partition between two pyroxenes and the host lava. *Earth Planet. Sci. Lett.* **5**, 47–51.

Papike J. J., Spilde M. N., Fowler G. W., and McCallum I. S. (1995) SIMS studies of planetary cumulates: orthopyroxene from the Stillwater Complex, Montana. *Amer. Mineral.* **80**, 1208–1221.

Papike J. J., Fowler G. W., Shearer C. K., and Layne G. D. (1996) Ion microprobe investigation of plagioclase and orthopyroxene from lunar Mg-suite norites: Implications for calculating parental melt REE concentrations and for assessing postcrystallization REE redistribution. *Geochim. Cosmochim. Acta* **60**, 3967–3978.

Peters M. T., Shaffer E. E., Burnett D. S., and Kim S. S. (1995) Magnesium and titanium partitioning between anorthite and Type B CAI liquid: Dependence on oxygen fugacity and liquid composition. *Geochim. Cosmochim. Acta* **59**, 2785–2796. **(P1)**

Petrov I., Agel A ., and Hafner S. S. (1989a) Distinct defect centers at oxygen positions in albite. *Amer. Mineral.* **74**, 1130–1341.

Petrov I., Bershov L.V., Hafner S. S., and Kroll H. (1989b) Order-disorder of Fe3+ ions over the tetrahedral positions in albite. *Amer. Mineral.* **74**, 604–609.

Philpotts J.A. (1978) The law of constant rejection. *Geochim. Cosmochim. Acta* **42**, 909–920.

Phinney W. C. (1992) Partition coefficients for iron between plagioclase and basalt as a function of oxygen fugacity; implication for Archean and lunar anorthosites. *Geochim. Cosmochim. Acta* **56**, 1885–1895. **(P2)**

Phinney W. C. and Morrison D. A. (1990) Partition coefficients for calcic plagioclase; implications for Archean anorthosites. *Geochim. Cosmochim. Acta* **54**, 1639–1654. **(P3)**

Sato H. (1989) Mg-Fe partitioning between plagioclase and liquid in basalts of hole 504B, ODP leg 111: a study of melting at 1 atm. *Proc. Ocean Drilling Program* **111**, 17–26. **(S3)**

Schnetzler C. C. and Philpotts J. A. (1970) Partition coefficients ements between igneous matrix material phenocrysts. *Geochim. Cosmochim. Acta* **34**, 307–340. **(S1)**

Shannon R. D. (1976) Revised effective ionic radii and systematic studies of interatomic distances in halides and chalcogenides. *Acta Cryst.* **A32**, 751–767.

Simon S. B., Grossman L., and Davis A. M. (1991) Fassaite composition trends during crystallization of Allende Type B refractory inclusion melts. *Geochim. Cosmochim. Acta* **55**, 2635–2655.

Simon S. B., Kuehner S. M., Davis A. M., Grossman L., Johnson M. L., and Burnett D. S. (1994) Experimental studies of trace element partitioning in Ca, Al-rich compositions: anorthite and perovskite. *Geochim. Cosmochim. Acta* **58**, 1507–1523. **(S2)**

Singer B. S., Dungan M. A., and Layne G. D. (1995) Textures and Sr, Ba, Mg, Fe, K, and Ti compositional profiles in volcanic plagioclase: clues to the dynamics of calc-alkaline magma chambers. *Amer. Mineral.* **80**, 776–798.

Smith J. V. and Brown W. L. (1988) *Feldspar Minerals.* Vol.1. Springer-Verlag.

Stolper E. (1975) Origin of the basaltic achondrites. *LSI Contribution* **234**, 154–158.

Vernieres J., Joron J.-L., Treuil M., Coulon C., and Dupuy C. (1977) Coefficient de partage de quelques elements en trace entre plagioclase et verre dans les ignimbrites—Implications petrogenetiques. *Chem. Geol.* **19**, 309–325. **(V1)**

Weill D. F. and Drake M.J. (1973) Europium anomaly in plagioclase feldspar: Experimental results and a semiquantitative model. *Science* **180**, 1059–1060.

Weill D. F. and McKay G. A. (1976) The partitioning of Mg, Fe, Sr, Ce, Sm, Eu, and Yb in lunar igneous systems and a possible origin of KREEP by equilibrium partial melting. *Proc. 6th Lunar Planet. Sci. Conf.*, 1143–1158. **(W1)**

Williamson J. H. (1968) Least-squares fitting of. *Canadian J. Phys.* **46**, 1845–1854.

Worner G., Beusen J. M., Duchateau N., Gijbels R., and Schmincke H.-U. (1983) Trace element abundances and mineral/melt distribution coefficients in Laacher See Volcano (Germany). *Contrib. Mineral. Petrol.* **84**, 152–173. **(W2)**

Yurimoto H. and Sueno S. (1984) Anion and cation partitioning between olivine, plagioclase phenocrysts and the host magma: a new application of ion microprobe study. *Geochem. J.* **18**, 85–94. **(Y1)**